Inorg. Chem. **2008**, *47*, 2280−2293

Molecular Architectures for Trimetallic d/f/d Complexes: Structural and Magnetic Properties of a $LnNi_2$ Core

Cheri A. Barta, Simon R. Bayly, Paul W. Read, Brian O. Patrick, Robert C. Thompson,* and Chris Orvig*

Department of Chemistry, University of British Columbia, 2036 Main Mall, Vancouver, British Columbia V6T 1Z1, Canada

Received August 13, 2007

A series of cationic, trimetallic d/f/d complexes have been prepared which use a multidentate, macrocyclic amine phenol ligand to coordinate divalent first row d-block transition metal ions (TM) and lanthanides (Ln) ions in close proximity, desirable for magnetic studies. Isolable complexes of the d/f/d cluster compounds with the formula $[Ln(TM)_2(bcn)_2]ClO_4 \cdot nH_2O$, where H_3bcn is tris-*N*,*N*′,*N*″-(2-hydroxybenzyl)-1,4,7-triazacyclononane, TM = Zn(II) and Ni(II) and Ln = La(III), Nd(III), Gd(III), Dy(III), and Yb(III), were synthesized by a one-pot sequential reaction of stoichiometric amounts of H_3bcn with the TM(II) and Ln(III) metal ions. The spontaneously formed cationic complexes were characterized by a variety of analytical techniques including IR, NMR, +ESI-MS, and EA. The $[TM(Hbcn)] \cdot nH_2O$ and $[TM_3(bcn)_2] \cdot nH_2O$ complexes were also synthesized to probe the building blocks of the d/f/d coaggregated species. The solid-state X-ray crystal structures of $[GdNi_2(bcn)_2(CH_3CN)_2]ClO_4 \cdot CH_3CN$ and $[GdZn_2(bcn)_2(CH_3CN)_2]ClO_4 \cdot CH_3CN$ were determined to be nearly identical with each TM(II) encapsulated in an octahedral geometry by the N_3O_3 binding pocket of the bcn^{3-} ligand. The eight coordinate Gd(III) was bicapped by two $[TM(bcn)]^-$ moieties and coordinated by two solvent molecules. Because of the isostructurality of the $[LnZn_2(bcn)_2]ClO_4 \cdot nH_2O$ and $[LnNi_2(bcn)_2]ClO_4 \cdot nH_2O$ complexes, an empirical approach using the $LnZn_2$ magnetic data was utilized to remove first-order anisotropic contributions from the $LnNi_2$ species. Ferromagnetic spin interactions were determined for the $[LnNi_2(bcn)_2]ClO_4 \cdot nH_2O$ complexes, where Ln = Gd(III), Dy(III), and Yb(III), while an antiferromagnetic exchange was observed for Ln = Nd(III).

Introduction

Currently, lanthanides are being explored in a myriad of areas including in medicine as MRI contrast agents,[1,2] radiotherapeutic drugs,[3,4] and fluorescent probes,[5] in catalysis for homogeneous carbon−carbon bond formation,[6] and in materials for fluorescent thin films and light-emitting diodes.[7,8] Lanthanides are also part of the most powerful permanent magnet known to date consisting of an Fe(II)/Nd(III) core;[9–11] however, the magnetic exchange between transition metal (TM) and lanthanide (Ln) ions is not well understood. Many obstacles, including the weak d/f interactions, the large anisotropic effects of Ln (except for La(III), Gd(III), and Lu(III)), and the challenge of designing a ligand that coordinates both d- and f-block transition metal ions in close proximity have contributed to the complexity of understanding this important magnetic exchange.

The existing magnetic studies on heterometallic d−f complexes have been mainly confined to Schiff base Cu−Gd systems[12–22] first studied by Gatteschi in 1985.[14] Only a handful of examples of Gd−Cu species in a range of

* To whom correspondence should be addressed. E-mail: thompson@chem.ubc.ca (R.C.T.); orvig@chem.ubc.ca (C.O.).

(1) Lauffer, R. B. *Chem. Rev.* **1987**, *87*, 901.
(2) Caravan, P.; Ellison, J. J.; McMurry, T. J.; Lauffer, R. B. *Chem. Rev.* **1999**, *99*, 2293.
(3) Cutler, C. S.; Smith, C. J.; Ehrhardt, G. J.; Tyler, T. T.; Jurisson, S. S.; Deutsch, E. *Cancer Biother. Radiopharm.* **2000**, *15*, 531.
(4) Fricker, S. P. *Chem. Soc. Rev.* **2006**, *35*, 524.
(5) Thunus, L.; Lejeune, R. *Coord. Chem. Rev.* **1999**, *184*, 125.
(6) Mikami, K.; Terada, M.; Matsuzawa, H. *Angew. Chem., Int. Ed.* **2002**, *41*, 3554.
(7) Bünzli, J.-C. G.; Piguet, C. *Chem. Soc. Rev.* **2005**, *34*, 1048.
(8) Kido, J.; Okamoto, Y. *Chem. Rev.* **2002**, *102*, 2357.
(9) Rauluszkiewicz, J.; Szymczak, H.; Lachowicz, H. K. *Physics of Magnetic Material*; World Scientific: Singapore, 1985.
(10) Coey, J. M. D. *Endeavour* **1995**, *19*, 146.
(11) Muller, K. H.; Krabbes, G.; Fink, J.; Gruss, S.; Kirchner, A.; Fuchs, G.; Schultz, L. J. *J. Magn. Magn. Mater.* **2001**, *226–230*, 1370.
(12) Costes, J.-P.; Dahan, F.; Dupuis, A. *Inorg. Chem.* **2000**, *39*, 5994.
(13) Ramade, I.; Kahn, O.; Jeannin, Y.; Robert, F. *Inorg. Chem.* **1997**, *36*, 930.

10.1021/ic701612e CCC: $40.75
Published on Web 03/05/2008

coordination environments[20,23–28] or other Cu−Ln complexes where Ln ≠ Gd, are known.[21,29–35] Systematic studies on the structure and magnetic properties of TM−Ln species, including Ni−Ln complexes, are even rarer.[36–43]

We have previously synthesized a variety of Ni(II)−Ln(III)−Ni(II) complexes using tripodal amine phenol ligands, H_3tam [1,1,1-tris(((2′-hydroxybenzyl)amino)methyl)ethane][36] and H_3trn, [tris(2′-hydroxybenzylaminoethyl)amine][41] to probe the magnetic interactions between d and f metal ions (Figure 1). Despite the similarities in the ligand structure, very different magnetic properties were observed between the two series of Ni−Ln−Ni species.[36,41] The $[LnNi_2(trn)_2]^+$ complexes exhibited a ferromagnetic exchange for Ln = Gd(III), Tb(III), Dy(III), Ho(III), and Er(III) (and possibly Tm(III) and Yb(III)), following the trend of other documented Ni−Ln species (a Ni_3Ln_2 ladder complex[44] and one Ni_2Ln cluster).[36,41,45] These results suggest that Kahn's prediction (stating that ferromagnetic couplings are observed for Ln(III) ions with f^7−f^{13} configurations in Cu(II)−Ln(III) systems)[44,46] may also be relevant for other TM(II)−Ln(III) species. Alternatively, however, antiferromagnetic interactions were observed for the $[LnNi_2(tam)_2]^+$ species where Ln = Dy(III) and Yb(III).[36] To probe these contrasting results, it was deemed necessary to design new ligands that cannot only afford discrete d−f mixed-metal complexes to better understand the effects of the geometric constraints on the observable magnetic exchange but also to synthesize systems where the TM can be varied to produce a series of diamagnetic and paramagnetic complexes in which the first-order orbital contributions of the Ln(III) can be removed.[21,29–35,47]

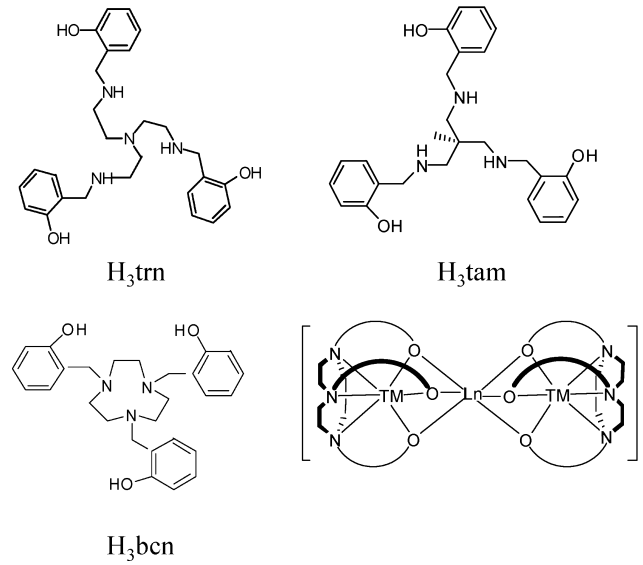

Figure 1. Ligands of interest and proposed binding motifs for the d/f/d heterometallic complexes.

Costes et al. were the first to synthesize a Ni−Ln system isostructural with a Cu−Ln species of interest,[31] where the Ni(II) was held in a square planar environment giving rise to a low-spin, diamagnetic state. When identical crystal-field effects are assumed for the two complexes, the magnetic behavior between the d−f metals for the Cu−Ln species could be unmasked by removal of the first-order orbital contributions of the Ln(III) determined from the Ni−Ln magnetic data. A similar method was used by Matsumoto,[35] Kahn,[32,34] Ōkawa[45,48] and co-workers to reduce the misinterpretation of the magnetic exchange between the d- and f-block metals.

Using a similar concept, we have synthesized a series of heterometallic d/f/d cluster compounds using a slightly more geometrically demanding trisubstituted macrocyclic amine phenol ligand, H_3bcn (tris-*N*,*N*′,*N*″-(2-hydroxybenzyl)-1,4,7-

(14) Bencini, A.; Benelli, C.; Caneschi, A.; Carlin, R. L.; Dei, A.; Gatteschi, D. J. *J. Am. Chem. Soc.* **1985**, *107*, 8128.
(15) Costes, J.-P.; Novitchi, G.; Shova, S.; Dahan, F.; Donnadieu, B.; Tuchagues, J.-P. *Inorg. Chem.* **2004**, *43*, 7792.
(16) Costes, J.-P.; Dahan, F.; Dupuis, A.; Laurent, J.-P. *Inorg. Chem.* **2000**, *39*, 169.
(17) Costes, J.-P.; Dahan, F.; Dupuis, A.; Laurent, J.-P. *Inorg. Chem.* **1996**, *35*, 2400.
(18) Andruh, M.; Ramade, I.; Codjovi, E.; Guillou, O.; Kahn, O.; Trombe, J. C. *J. Am. Chem. Soc.* **1993**, *115*, 1822.
(19) Akine, S.; Taniguchi, T.; Nabeshima, T. *Angew. Chem., Int. Ed.* **2002**, *41*, 4670.
(20) Ghoerghe, R.; Andruh, M.; Costes, J.-P.; Donnadieu, B. *Chem. Commun.* **2003**, 2778.
(21) Guillou, O.; Oushoorn, R. L.; Kahn, O.; Baubekeur, K.; Batail, P. *Angew. Chem., Int. Ed. Eng.* **1992**, *31*, 626.
(22) Costes, J.-P.; Dahan, F.; Dupuis, A.; Laurent, J.-P. *Inorg. Chem.* **1997**, *36*, 3429.
(23) Gao, S.; Yang, Y.; Xu, G. *J. Alloys Compd.* **1995**, *225*, 234.
(24) Winpenny, R. E. P. *Chem. Soc. Rev.* **1998**, *27*, 447.
(25) Sakamoto, M.; Manseki, K.; Ōkawa; H., *Coord. Chem. Rev.* **2001**, *219–221*, 379.
(26) Benelli, C.; Gatteschi, D. *Chem. Rev.* **2002**, *102*, 2369.
(27) Shiga, T.; Ohba, M.; Ōkawa, H. *Inorg. Chem. Commun.* **2003**, *6*, 15.
(28) Benelli, G.; Caneschi, A.; Gatteschi, D.; Guillou, O.; Pardi, L. *Inorg. Chem.* **1990**, *29*, 1750.
(29) Stemmler, A. J.; Kampt, J. W.; Kirk, M. L.; Atasi, B. H.; Pecoraro, V. L. *Inorg. Chem.* **1999**, *38*, 2807.
(30) He, F.; Tong, M.-L.; Chen, X.-M. *Inorg. Chem.* **2005**, *44*, 559.
(31) Costes, J.-P.; Dahan, F.; Dupuis, A.; Laurent, J.-P. *Chem.—Eur. J.* **1998**, *4*, 1616.
(32) Kahn, M. L.; Mathoniere, C.; Kahn, O. *Inorg. Chem.* **1999**, *38*, 3692.
(33) Costes, J.-P.; Auchel, M.; Dahan, F.; Peyrou, V.; Shova, S.; Wernsdorfer, W. *Inorg. Chem.* **2006**, *45*, 924.
(34) Osa, S.; Kido, T.; Matsumoto, N.; Re, N.; Pochaba, A.; Mrozinski, J. *J. Am. Chem. Soc.* **2003**, *126*, 420.
(35) Kido, T.; Ikuta, Y.; Suantsuki, Y.; Ogawa, Y.; Matsumoto, N. *Inorg. Chem.* **2003**, *42*, 398.
(36) Xu, Z.; Read, P. W.; Hibbs, D. E.; Hursthouse, M. B.; Malik, K. M. A.; Patrick, B. O.; Rettig, S. J.; Seid, M.; Summers, D. A.; Pink, M.; Thompson, R. C.; Orvig, C. *Inorg. Chem.* **2000**, *39*, 508.
(37) Yamaguchi, T.; Sunatsuki, Y.; Kojima, M.; Akashi, H.; Tsuchimoto, M.; Re, N.; Osa, S.; Matsumoto, N. *Chem. Commun.* **2004**, 1048.
(38) Yue, Q.; Yang, J.; Li, G.-H.; Li, G.-D.; Xu, W.; Chen, J.-S.; Wang, S.-N. *Inorg. Chem.* **2005**, *44*, 5241.
(39) Lisowski, J.; Starynowicz, P. *Inorg. Chem.* **1999**, *38*, 1351.
(40) Costes, J.-P.; Dahan, F.; Dupuis, A.; Laurent, J.-P. *Inorg. Chem.* **1997**, *36*, 4284.
(41) Bayly, S. R.; Xu, Z.; Patrick, B. O.; Rettig, S. J.; Pink, M.; Thompson, R. C.; Orvig, C. *Inorg. Chem.* **2003**, *42*, 1576.
(42) Chen, Q.-Y.; Luo, Q.-H.; Zheng, L.-M.; Wang, Z.-L.; Chen, J.-T. *Inorg. Chem.* **2002**, *41*, 605.
(43) Pointillart, F.; Bernot, F.; Sessoli, R.; Gatteschi, D. *Chem.—Eur. J.* **2007**, *13*, 1602.
(44) Kahn, M. L.; Lecante, P.; Verelst, M.; Mathoniere, C.; Kahn, O. *Chem. Mater.* **2000**, *12*, 3073.
(45) Shiga, T.; Ito, N.; Hidaka, A.; Ōkawa, H.; Kitagawa, S.; Ohba, M. *Inorg. Chem.* **2007**, *46*, 3492.
(46) Kahn, O.; Guillou, O. *Research Frontiers in Magnetism*; O'Connor, C. J., Ed.; World Scientific: London, 1993.
(47) Li, Y.-T.; Yan, C.-W.; Zhang, J. *Cryst. Growth Des.* **2002**, *3*, 481.
(48) Shiga, T.; Ohba, M.; Ōkawa, H. *Inorg. Chem.* **2004**, *43*, 4435.

Scheme 1. Synthesis of H_3bcn[a]

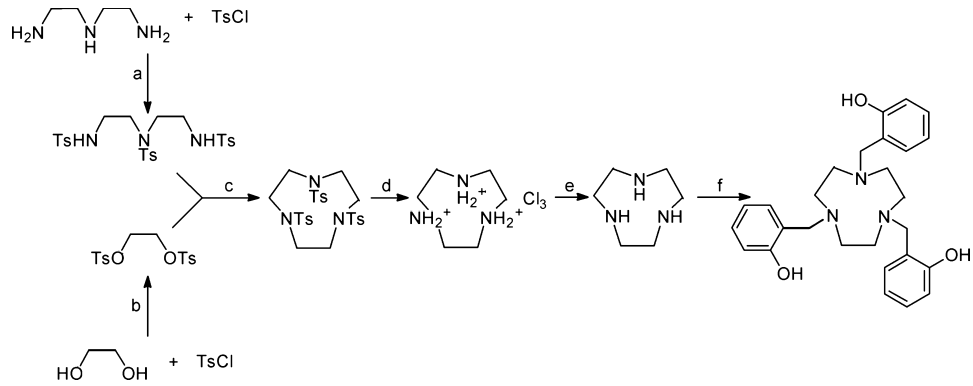

[a] Ts = *p*-$CH_3C_6H_4SO_2$. Reaction conditions: (a) NaOH, H_2O/ether, RT, 70%; (b) pyridine, O°C, Ar, 50%; (c) anhydrous DMF, 60% NaH, 70°C, Ar, 94%; (d) conc. H_2SO_4, 160°C, Ar; (e) H_2O/NaOH, CH_3Cl, RT, 72%; (f) dry EtOH, salicylaldehyde, $NaBH(OAc)_3$, RT, Ar, 82%.

triazacyclononane)[49] to probe the effects of the geometric constraints on the magnetic properties of d/f/d complexes (Figure 1). H_3bcn has three moderately hard amine donors that can preferentially accommodate divalent d-block transition metals and three very hard phenolate donors used to chelate harder trivalent f-block metals.

The synthesis and characterization of the geometrically more demanding H_3bcn ligand and its subsequent $[TM(Hbcn)]\cdot nH_2O$, $[TM_3(bcn)_2]\cdot nH_2O$, and $[LnTM_2(bcn)_2]ClO_4\cdot nH_2O$ complexes are discussed herein, where TM = Zn(II) and Ni(II) and Ln = La(III), Nd(III), Gd(III), Dy(III), and Yb(III). An empirical determination of the magnetic interactions between the different metal species can be elucidated by using the analogous diamagnetic La(III) or Zn(II) species, similar to the analyses by Costes,[31] Kahn,[32,44] Ōkawa,[45,48] Matsumoto[35] and co-workers. The examination of the magnetic properties of these species allows for a comprehensive study on the effects of the varied geometric, spin, and orbital contributions on the overall magnetic behavior between d and f metals using similar amine phenol ligands. In addition, the procedures used herein can be translated to the magnetic analysis of other d/f/d systems including the $[LnCu_2(bcn)_2]ClO_4\cdot nH_2O$ species fully characterized in the following paper.[50]

Experimental Section

Materials. Reagents were purchased from commercial sources and were used without purification unless otherwise stated. Hydrated Ln(III) perchlorate salts were obtained from Alfa Aesar as 50% (w/w) solutions in water and evaporated to dryness. Triethylamine was purchased from Fisher Scientific and used as received. NMR solvents were obtained from Sigma-Aldrich and were used as received. Methanol, ethanol, and acetonitrile were dried over activated 4 Å molecular sieves prior to use. Water was deionized (Barnstead D8902 and D8904 Cartridges) and distilled (Hytrex II GX50-9-7/8 and GX100-9-7/8) before use. Yields for the analytically pure compounds were calculated on the basis of the respective metal ion starting material.

Caution!. *Perchlorate salts are potentially explosive and should be handled with extreme care and used only in small quantities.*

Physical Measurements. ^1H NMR spectra were recorded on a Bruker Avance 300 spectrometer (300 MHz) or a Bruker Avance 400 inverse spectrometer (400 MHz) at room temperature (RT) and were calibrated with listed deuterated solvents. Infrared spectra were recorded as nujol mulls (KBr windows) in the range 4000–500 cm^{-1} on a Mattson Galaxy Series FTIR-5000 spectrophotometer and were referenced to polystyrene (1601 cm^{-1}). Elemental analyses of C, H, and N were performed by Mr. M. Lakha at the University of British Columbia (UBC). UV–vis spectra were recorded in methanol using a Hewlett-Packard 8543 diode array spectrophotometer and a 1 cm cuvette. Mass spectra were obtained on a Bruker Esquire ion trap (electrospray ionization mass spectrometry, ESI-MS) spectrophotometer. Approximately 1 mg of sample was dissolved in 1 mL of methanol or acetonitrile for +ESI-MS analysis. Room-temperature magnetic susceptibilities on powdered samples of $H_3[Ni(bcn)]_2ClO_4$, $[Ni(Hbcn)]\cdot H_2O$, and $[Ni_3(bcn)_2]\cdot 2H_2O$ complexes were measured on a Johnson Matthey MSB-1 balance standardized with $CoCl_2\cdot 6H_2O$ and $CuSO_4\cdot 5H_2O$. Variable-temperature and applied-field magnetic susceptibility measurements for all other powdered samples were performed on a Quantum Design MPMS XL SQUID magnetometer over the temperature range of 2−300 K at 10 000 and 500 G at UBC. Diamagnetic corrections for the constituent atoms used Pascal's constants[51] (6.10×10^{-4} $cm^3\ mol^{-1}$ per mole of complex, plus 3.89×10^{-5} $cm^3\ mol^{-1}$ per water). A specially designed sample holder, as described previously,[52] was used to minimize the background signal. Magnetic susceptibilities were corrected for the background signal generated by the holder.

Ligand Synthesis. 1,4,7-Triazacyclononane was synthesized using a significant modification of a published procedure.[53]

Diethylene-1,4,7-triamine Tritosylate. Diethylenetriamine (8.26 g, 0.08 mol) and NaOH (9.6 g, 0.24 mol) were dissolved in 80 mL of water. The solution was added dropwise to *p*-toluenesulfonyl chloride (TsCl, 45.6 g, 0.24 mol) dissolved in 240 mL diethyl ether. After the mixture was continuously stirred for 2 h at RT, the off-white product was filtered and washed with water and diethyl ether. The resulting white solid was vaccuum-dried without further purification to yield 30 g, 70%. ^1H NMR (300 MHz, RT, $(CD_3)_2CO$): δ 7.75 (d, 4H, ^3J = 8.2 Hz, aromatic C*H*), 7.64 (d, 2H, aromatic C*H*, ^3J = 8.3 Hz), 7.41 (d, 4H, aromatic C*H*, ^3J = 9.2 Hz), 7.39 (d, 2H, aromatic C*H*, ^3J = 8.01 Hz), 6.56 (t, 2H, N*H*, ^3J

(49) Auerbach, U.; Eckert, U.; Wieghardt, K.; Nuber, B.; Weiss, J. *Inorg. Chem.* **1990**, *29*, 938.
(50) Barta, C. A.; Bayly, S. R.; Read, P. W.; Patrick, B. O.; Thompson, R. C.; Orvig, C. *Inorg. Chem.* **2008**, *47*, 2294–2302.
(51) Pascal, P. *Chimie Generale*; Masson et Cie: Paris, 1949.
(52) Ehlert, M. K.; Rettig, S. J.; Storr, A.; Thompson, R. C.; Trotter, J. *Can. J. Chem.* **1991**, *69*, 432.
(53) Richman, J. E.; Atkins, T. J. J. *J. Am. Chem. Soc.* **1974**, *96*, 2268.

Table 1. List of the $[LnTM_2(bcn)_2]ClO_4 \cdot nH_2O$ Complexes Prepared and Their Analytical Data

	%C		%H		%N		
complex	found	calcd	found	calcd	found	calcd	+ESI-MS (*m*/*z*)
$[LaZn_2(bcn)_2]ClO_4 \cdot 4H_2O$	48.90	48.76	4.82	5.15	6.81	6.32	1157
$[NdZn_2(bcn)_2]ClO_4 \cdot 3H_2O$	49.08	49.23	5.11	5.05	6.52	6.38	1163
$[GdZn_2(bcn)_2]ClO_4 \cdot H_2O$	50.06	50.10	5.20	4.83	6.68	6.49	1176
$[DyZn_2(bcn)_2]ClO_4 \cdot H_2O$	50.79	50.60	5.12	4.72	6.96	6.56	1181
$[YbZn_2(bcn)_2]ClO_4 \cdot H_2O$	50.58	50.19	4.87	4.68	6.45	6.50	1192
$[LaNi_2(bcn)_2]ClO_4 \cdot 3H_2O$	49.71	49.93	5.25	5.12	6.51	6.47	1145
$[NdNi_2(bcn)_2]ClO_4 \cdot 2H_2O$	49.14	49.28	4.79	4.75	6.18	6.39	1150
$[GdNi_2(bcn)_2]ClO_4 \cdot H_2O$	50.41	50.62	4.91	4.88	6.89	6.56	1163
$[DyNi_2(bcn)_2]ClO_4 \cdot H_2O$	50.04	49.84	5.02	4.72	6.32	6.46	1169
$[YbNi_2(bcn)_2]ClO_4$	50.76	50.71	4.79	4.73	6.71	6.57	1179

= 5.82 Hz), 3.20 (tt, 4H, CH_2, ^3J = 7.53 Hz, ^2J = 3.18 Hz), 3.06 (tt, 4H, CH_2, ^3J = 7.53 Hz, ^2J = 3.09 Hz), 2.43 (s, 6H, CH_3), 2.42 (s, 3H, CH_3). ^{13}C NMR (75.5 MHz, RT, $(CD_3)_2CO$): δ 144.07 (2*C*), 138.87 (2*C*), 130.76, 130.61, 128.18, 127.94, 50.28, 43.18, 21.48 (2*C*). MS (+ESI): *m*/*z* 588 ([L + Na]$^+$).

Ethyleneglycol Ditosylate. Over 30 min, small portions of TsCl (114 g, 0.6 mol) were slowly added to ethylene glycol (18.6 g, 0.3 mol) dissolved in 500 mL of pyridine under Ar and cooled to 0 °C using an ice bath. After it was continuously stirred at 0 °C under Ar for 5 h, the solution was poured onto crushed ice (~500 mL) and acidified using concentrated HCl until pH 1 (~700 mL of HCl). The white precipitate was washed with cold water, recrystallized from hot methanol, and dried for 48 h in vacuo to yield 50 g, 50%. ^{1}H NMR (300 MHz, RT, CD_3Cl): δ 7.71 (d, 4H, aromatic C*H*, ^3J = 6.6 Hz), 7.32 (d, 4H, aromatic C*H,* ^3J = 8.0 Hz), 4.17 (s, 4H, CH_2), 2.43 (s, 6H, CH_3). ^{13}C NMR (75.5 MHz, RT, $CDCl_3$): δ 145.46, 132.40, 130.13, 128.08, 66.92, 21.81. MS (+ESI): *m*/*z* 393 ([L + Na]$^+$).

1,4,7-Triazacyclononane Tristosylate. Diethylene-1,4,7-triamin-etritosylate (24.1 g, 0.0427 mol) was dissolved in 100 mL of anhydrous DMF dried over 4 Å sieves. Small portions of 60% NaH in oil (previously rinsed with petroleum ether, 6 g, 0.25 mol) were slowly added. The reaction was heated to 70 °C under Ar. After the mixture had been continuously stirred for 30 min, a solution of ethyleneglycol ditosylate (15.8 g, 0.0427 mol) in dry DMF (200 mL) was added dropwise over a 5 h period. The solution was stirred for 20 h under Ar at 70 °C, after which the reaction volume was reduced to ~200 mL under reduced pressure and slowly added to ~1000 mL ice and water affording a yellow precipitate. The solution was stored at 4 °C for 5 h before filtration; the filtrate was washed with water, ethanol, and ether, dried in vacuo overnight, and used without further purification to yield 24.1 g, 94%. ^{1}H NMR (300 MHz, RT, CD_3Cl): δ 7.69 (d, 6H, aromatic C*H*, ^3J = 8.1 Hz), 7.32 (d, 6H, aromatic C*H*, ^3J = 8.1 Hz), 3.42 (s, 12H, CH_2), 2.43 (s, 9H, CH_3). ^{13}C NMR (75.5 MHz, RT, $CDCl_3$): δ 143.88, 132.57, 129.86, 127.47, 51.86, 21.51. MS (+ESI): *m*/*z* 614 ([L + Na]$^+$).

1,4,7-Triazacyclononane·Trihydrochlorate (tacn·3HCl). 1,4,7-Triazacyclonone tritosylate (24.1 g, 0.0407 mol) was added to 40 mL of concentrated H_2SO_4. The brown slurry was heated at 160 °C for 30 min under Ar and allowed to cool to RT before being added dropwise to cold EtOH (200 mL), followed by 300 mL of diethyl ether. After storage at 4 °C overnight, the brown precipitate was filtered, dissolved in 150 mL of H_2O, and decolorized by boiling the solution for 15 min in the presence of Norit and Celite. After the solution was clarified by filtration, the solvent was removed under reduced pressure to afford a light brown oil. An off-white precipitate immediately formed upon the addition of 25 mL of concentrated HCl, followed by 150 mL of ethanol. The solid was filtered, washed with ethanol and ether, and recrystallized from H_2O/EtOH (1:8) to yield 9.2 g, 95%. ^{1}H NMR (300 MHz, RT, D_2O): δ 3.43 (s, 12H, CH_2). ^{13}C NMR (75.5 MHz, RT, D_2O/CD_3OD): δ 45.78.

1,4,7-Triazacyclononane (tacn). Tacn·3HCl (9.2 g, 0.0388 mol) was dissolved in 20 mL of deionized H_2O. The pH was adjusted to ~13 by addition of NaOH pellets (~4.3 g, 2.8 equiv), and the product was extracted into chloroform by continuous extraction for 48 h. The chloroform layer was removed, and the aqueous layer was further extracted with chloroform (3 × 30 mL). The combined chloroform layers were dried over $NaSO_4$ and filtered. The solvent was removed under reduced pressure, affording a pale yellow oil to yield 3.6 g, 72%. ^{1}H NMR (300 MHz, RT, D_2O): δ 2.78 (s, 12H, CH_2). ^{13}C NMR (75.5 MHz, RT, D_2O/CD_3OD): δ 46.92. MS (+ESI): *m*/*z* 130 ([L + H]$^+$). MS (+ESI, high-res.) calcd for $C_6H_{16}N_3$: 130.1344. Found: 130.1347.

***N*,*N*′,*N*″-Tris(2-hydroxybenzyl)-1,4,7-triazacyclononane (H_3bcn).** To a solution of tacn (3.1 g, 0.0279 mol) in dry ethanol was added salicylaldehyde (10.22 g, 0.0837 mol) dropwise. The solution was allowed to stir for 2 h under Ar before the solvent was removed under reduced pressure, leaving an orange oil. The oil was dissolved in dry dichloromethane under Ar, followed by the slow addition of $NaBH(OAc)_3$ (35.48 g, 0.1674 mol) over a period of 3 h. The white cloudy solution was allowed to stir for an additional 3 h under Ar after which excess $NaBH(OAc)_3$ was quenched by the addition of a saturated solution of sodium bicarbonate. The product was extracted from the aqueous layer with chloroform (3 × 50 mL) and dried over $MgSO_4$, and the volatiles were removed in vacuo. The product was recrystallized in MeOH/H_2O yielding an off white solid that was obtained in excellent yield with respect to tacn, 10.23 g, 82%. ^{1}H NMR (300 MHz, RT, $CDCl_3$): δ 7.19 (t, 3H, aromatic C*H*, ^3J = 7.8 Hz), 6.93 (d, 3H, aromatic C*H*, ^3J = 7.2 Hz), 6.90 (d, 3H, aromatic C*H*, ^3J = 7.2 Hz), 6.76 (t, 3H, aromatic C*H*, ^3J = 7.5 Hz), 3.77 (s, 6H, BnCH_2), 2.43 (s, 12H, CH_2). ^{1}H NMR (300 MHz, RT, CD_3OD): δ 7.22 (t, 3H, aromatic C*H*, ^3J = 8.1 Hz), 7.16 (d, 3H, aromatic C*H*, ^3J = 7.2 Hz), 6.87 (t, 3H, aromatic C*H*, ^3J = 8.1 Hz), 6.84 (d, 3H, aromatic C*H*, ^3J = 7.2 Hz), 3.86 (s, 6H, BnCH_2), 2.85 (s, 12H, CH_2). ^{13}C NMR (75.5 MHz, RT, CD_3OD): δ 164.18, 133.15, 131.07, 123.33, 120.79, 117.10, 60.50, 51.89. MS (+ESI): *m*/*z* 448 ([L + H]$^+$). Anal. Calcd (found) for $C_{27}H_{33}N_3O_3$: C, 72.46 (72.34); H, 7.43 (7.34); N, 9.39 (9.64).

Synthesis of Complexes. See Table 1 for a list of the $[LnTM_2(bcn)_2]ClO_4 \cdot nH_2O$ species prepared and their characterization data.

[Ni(Hbcn)]·H_2O. To a solution of H_3bcn (27.9 mg, 0.062 mmol) in 20 mL methanol was added $Ni(ClO_4)_2 \cdot 6H_2O$ (22.9 mg, 0.062 mmol). The pale yellow solution turned cloudy immediately after the addition. After the solution was stirred for 1 h, the yellow powder was filtered, washed with cold methanol, and air-dried to yield 16.9 mg, 54%. ^{1}H NMR (300 MHz, RT, CD_3OD): δ 7.14 (m, 6H, *o*-benzyl *H* and *m*-phenol *H*), 6.83 (m, 6H, *o*-phenol *H* and *p*-phenol *H*), 3.82 (s, br, 6H, benzyl CH_2, $\upsilon_{1/2}$ = 20 Hz,), 2.79

Scheme 2. Synthesis of $[LnTM_2(bcn)_2]^{+a}$

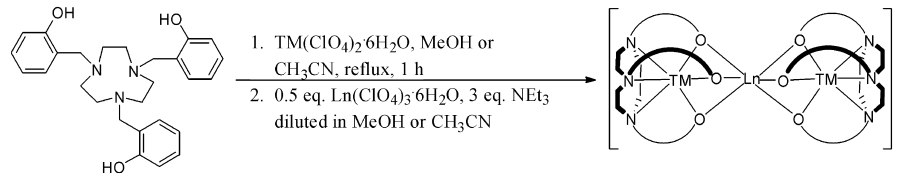

[a] TM = Ni(II) or Zn(II) and Ln = La(III), Nd(III), Gd(III), Dy(III), or Yb(III).

(m, 12H, CH_2). MS (+ESI): *m*/*z* 505 ([TM(HL) + H]$^+$). μ_{eff}: diamagnetic. Anal. Calcd. (found) for $C_{27}H_{33}N_3NiO_4$: C, 62.09 (62.34); H, 6.37 (6.26); N, 8.05 (8.30).

H_3[Ni(bcn)]$_2$ClO$_4$. To a solution of H_3bcn (27.9 mg, 0.062 mmol) in 20 mL acetonitrile was added $Ni(ClO_4)_2 \cdot 6H_2O$ (27.9 mg, 0.062 mmol). The solution turned a golden yellow color immediately after the addition and was stirred for 1 h at RT. The solution was filtered through glass wool and allowed to stand at RT, upon which purple needle crystals deposited. The crystals were filtered off, washed with cold water, and air-dried to yield 6.6 mg, 21%. ^{1}H NMR (300 MHz, RT, CD_3OD) is uninformative. MS (+ESI): *m*/*z* 505 ([TM(HL) + H]$^+$). μ_{eff}: 2.77 μ_B. Anal. Calcd (found) for $C_{54}H_{63}ClN_6Ni_2O_{10}$: C, 58.49 (58.14); H, 5.81 (5.89); N, 7.46 (7.67).

[Zn(Hbcn)]·H$_2$O. To a solution of H_3bcn (27.9 mg, 0.062 mmol) in methanol was added $Zn(ClO_4)_2 \cdot 6H_2O$ (23.1 mg, 0.062 mmol). The pale yellow solution became clear immediately after the addition and was continuously stirred for 1 h at RT. Evaporation of the solvent to ~2 mL afforded a white precipitate which was filtered, washed with cold methanol, and air-dried to yield 25.9 mg, 82%. ^{1}H NMR (300 MHz, RT $CDCl_3$): δ 7.14 (d, 3H, *o*-benzyl *H*, ^3J = 7.2 Hz), 6.98 (t, 3H, *m*-phenol *H*, ^3J = 7.2 Hz), 6.78 (t, 3H, *p*-phenol *H*, ^3J = 7.2 Hz), 6.14 (d, 3H, *o*-phenol *H*, ^3J = 7.2 Hz), 4.23 (d, 3H, benzyl CH_2, ^2J = 11.4 Hz), 3.39 (d, 3H, benzyl CH_2, ^2J = 11.4 Hz), 2.96 (ddd, 3H, CH_2, ^2J = 15.0 Hz, ^3J = 14.1 Hz, ^3J = 3.9 Hz), 2.66 (dd, 3H, CH_2, ^2J = 15.3 Hz, ^3J = 5.4 Hz), 2.31 (dd, 3H, CH_2, ^2J = 12.5 Hz, ^3J = 3.9 Hz), 1.97 (ddd, 3H, CH_2, ^2J = 12.8 Hz,^3J = 12.3 Hz, ^3J = 6.0 Hz). MS (+ESI): *m*/*z* 511 ([TM(HL) + H]$^+$). Anal. Calcd (found) for $C_{27}H_{33}N_3O_4Zn$: C, 61.31 (61.02); H, 6.29 (6.30); N, 7.94 (8.20).

[Ni$_3$(bcn)$_2$]·2H$_2$O. To a solution of H_3bcn (27.9 mg, 0.062 mmol) in methanol was added $Ni(ClO_4)_2 \cdot 6H_2O$ (22.9 mg, 0.062 mmol). The pale yellow solution immediately turned clear following the addition. The solution was refluxed for 1 h and allowed to cool before addition of the third equivalent of $Ni(ClO_4)_2 \cdot 6H_2O$ (11.4 mg, 0.031 mmol). The solution was allowed to stir at RT for 30 min before NEt_3 (18.8 mg, 0.186 mmol) was added dropwise. The solvent was evaporated to ~2 mL. A light purple precipitate formed after additional solvent was slowly evaporated. The powder was filtered, washed with cold methanol, and air-dried to yield 28.4 mg, 43%. MS (+ESI): *m*/*z* 1065 ([TM$_3$L$_2$ + H]$^+$). μ_{eff} : 5.54 μ_B. Anal. Calcd (found) for $C_{54}H_{64}N_6Ni_3O_8$: C, 58.90 (59.29); H, 5.86 (5.84); N, 7.63 (7.83).

[Zn$_3$(bcn)$_2$]. To a solution of H_3bcn (27.9 mg, 0.062 mmol) in methanol was added $Zn(ClO_4)_2 \cdot 6H_2O$ (23.1 mg, 0.062 mmol). The pale yellow solution immediately turned clear following the addition. The solution was refluxed for 1 h and allowed to cool before addition of the third equivalent of $Zn(ClO_4)_2 \cdot 6H_2O$ (11.6 mg, 0.031 mmol). The solution was allowed to stir at RT for 30 min before NEt_3 (18.8 mg, 0.186 mmol) was added dropwise. A white precipitate formed after the solvent was evaporated to ~2 mL which was filtered, washed with cold methanol, and air-dried to yield 37.7 mg, 56%. ^{1}H NMR (300 MHz, RT, $CDCl_3$): δ 7.13 (d, 6H, *o*-benzyl *H*, ^3J = 6.4 Hz), 6.98 (t, 6H, *m*-phenol *H*,^3J = 7.7), 6.78 (t, 6H, *p*-phenol *H*,^3J = 7.8 Hz), 6.13 (d, 6H, *o*-phenol *H*, ^3J = 8.2 Hz), 4.23 (d, 6H, benzyl CH_2, ^2J = 10.8 Hz), 3.39 (d, 6H, benzyl CH_2, ^2J = 12.0 Hz), 3.07 (ddd, 6H, CH_2, ^2J = 16.2 Hz, ^3J(A,B) = 15.0 Hz, ^3J = 2.7 Hz), 2.65 (dd, 6H, CH_2, ^2J = 15.06 Hz, ^3J = 3.9 Hz), 2.34 (dd, 6H, CH_2, ^2J = 12.3 Hz, ^3J = 3.6 Hz), 1.96 (ddd, 6H, CH_2, ^2J = 13.5 Hz, ^3J = 12.3 Hz, ^3J = 5.4 Hz). MS (+ESI): *m*/*z* 1085 ([TM$_2$L$_3$ + H]$^+$). Anal. Calcd (found) for $C_{54}H_{60}N_6O_6Zn_3$: C, 59.76 (59.80); H, 5.57 (5.72); N, 7.74 (7.89).

General Procedure for [LnNi$_2$(bcn)$_2$]ClO$_4$·*n*H$_2$O, Ln(III) = La, Nd, Gd, Dy, Yb (Scheme 2). To a solution of $Ni(ClO_4)_2 \cdot 6H_2O$ (91.4 mg, 0.25 mmol) in acetonitrile was added H_3bcn (111.9 mg, 0.25 mmol). A blue-green precipitate formed immediately in the pale yellow solution. The reaction was refluxed and allowed to stir for 1 h. Hydrated $Ln(ClO_4)_3 \cdot 6H_2O$ (68.2–72.4 mg, 0.125 mmol) was added after the solution was cooled to RT, affording a pale purple solution. The solution was stirred for an additional 30 min at RT before NEt_3 (75.6 mg, 0.75 mmol) diluted in 5 mL acetonitrile was added dropwise. After it was stirred for 5 min, the solution turned yellow. Pale purple powder deposited upon slow evaporation of the solvent (except in the case of $[GdNi_2(bcn)_2]ClO_4$ and $[YbNi_2(bcn)_2]ClO_4$ where prismatic purple crystals formed). The solid was filtered, washed with cold acetonitrile, and dried in air yielding 45–85%. ^{1}H NMR (300 MHz, RT, CD_3OD) was uninformative.

General Procedure for [LnZn$_2$(bcn)$_2$]ClO$_4$·*n*H$_2$O, Ln(III) = La, Nd, Gd, Dy, Yb. To a solution of H_3bcn (111.9 mg, 0.25 mmol) in methanol was added $Zn(ClO_4)_2 \cdot 6H_2O$ (93.1 mg, 0.25 mmol). The pale yellow solution immediately turned clear upon addition of the metal salt. The solution was refluxed and allowed to stir for 1 h. The hydrated $Ln(ClO_4)_3 \cdot 6H_2O$ (68.2 – 72.4 mg, 0.125 mmol) was added to the solution after it had cooled to RT. The clear solution was stirred for 30 min at RT and NEt_3 (75.6 mg, 0.75 mmol) diluted in 5 mL methanol was added dropwise. The solution turned slightly yellow after stirring for an additional five minutes. An off-white perchlorate salt deposited upon slow evaporation of the solvent (except in the case of $[GdZn_2(bcn)_2]ClO_4$ which was redissolved in acetonitrile and formed prismatic colorless crystals upon slow evaporation of the solvent) and was filtered, washed with cold ethanol, and dried in air yielding 60–85%. ^{1}H NMR for $[LaZn_2(bcn)_2]ClO_4$ (400 MHz, RT, $CDCl_3$, Supporting Information): δ 7.12 (d, 6H, *o*-benzyl *H*, ^3J = 6.2 Hz), 6.96 (t, 6H, *m*-phenol *H*, ^3J = 7.1 Hz), 6.75 (t, 6H, *m*-phenol *H*, ^3J = 7.3 Hz), 6.12 (d, 6H, *o*-phenol *H*, ^3J = 8.1 Hz), 4.20 (d, 6H, benzyl CH_2, ^2J = 11.7 Hz), 3.37 (d, 6H, benzyl CH_2, ^2J = 11.7 Hz), 2.95 (ddd, 6H, CH_2, ^2J = 16.0 Hz, ^3J = 14 Hz, ^3J = 3.9 Hz), 2.64 (dd, 6H, CH_2, ^2J = 15.5 Hz, ^3J = 5.32 Hz), 2.30 (dd, 6H, CH_2, ^2J = 12.5 Hz, ^3J = 4.3 Hz), 1.95 (ddd, 6H, CH_2, ^2J = 12.8 Hz, ^3J = 12.0 Hz, ^3J = 5.5 Hz). ^{13}C NMR (75 MHz, RT, CD_3OD): δ 167.02 (ring *C*−OH), 132.41 (*m*-*C*), 131.16 (*o*-benzyl *C*), 125.05 (benzyl *C*), 121.92 (*p*-phenol *C*), 116.83 (*o*-phenol *C*), 63.48 (benzyl *C*H$_2$), 57.64 (*C*H$_2$).

X-ray Crystallographic Analyses. Single crystals of the perchlorate salts of $H_3[Ni(bcn)]_2ClO_4 \cdot 3CH_3CN$, $[YbNi_2(bcn)_2]ClO_4 \cdot CH_3CN$, and $[GdZn_2(bcn)_2(CH_3CN)_2]ClO_4 \cdot CH_3CN$, isolated by

Table 2. Selected Bond Lengths (Å) and Angles (deg) in $H_3[Ni(bcn)]_2ClO_4 \cdot 3CH_3CN$

N(1)−Ni(1)	2.133(3)	O(3)−Ni(1)	1.987(4)
N(2)−Ni(1)	2.125(3)	O(4)−Ni(2)	2.028(3)
N(3)−Ni(1)	2.181(3)	O(5)−Ni(2)	1.991(3)
N(4)−Ni(2)	2.086(3)	O(6)−Ni(2)	2.104(3)
N(5)−Ni(2)	2.210(3)	O(7)−Cl(1)	1.433(3)
N(6)−Ni(2)	2.138(3)	O(8)−Cl(1)	1.423(4)
O(1)−Ni(1)	2.034(4)	O(9)−Cl(1)	1.420(3)
O(2)−Ni(1)	2.075(4)	O(10)−Cl(1)	1.378(3)
O(3)−Ni(1)−O(1)	87.28(17)	O(5)−Ni(2)−O(4)	86.44(17)
O(3)−Ni(1)−O(2)	84.15(17)	O(5)−Ni(2)−N(4)	168.43(16)
O(1)−Ni(1)−O(2)	85.29(17)	O(4)−Ni(2)−N(4)	89.13(12)
O(3)−Ni(1)−N(2)	100.25(17)	O(5)−Ni(2)−O(6)	87.77(15)
O(1)−Ni(1)−N(2)	170.93(15)	O(4)−Ni(2)−O(6)	85.96(14)
O(2)−Ni(1)−N(2)	90.42(13)	N(4)−Ni(2)−O(6)	102.58(15)
O(3)−Ni(1)−N(1)	171.12(15)	O(5)−Ni(2)−N(6)	102.17(17)
O(1)−Ni(1)−N(1)	89.64(13)	O(4)−Ni(2)−N(6)	169.49(14)
O(2)−Ni(1)−N(1)	103.90(17)	N(4)−Ni(2)−N(6)	83.50(11)
N(2)−Ni(1)−N(1)	83.63(13)	O(6)−Ni(2)−N(6)	88.34(11)
O(3)−Ni(1)−N(3)	93.31(13)	O(5)−Ni(2)−N(5)	88.08(12)
O(1)−Ni(1)−N(3)	102.33(17)	O(4)−Ni(2)−N(5)	102.73(15)
O(2)−Ni(1)−N(3)	171.87(15)	N(4)−Ni(2)−N(5)	82.47(11)
N(2)−Ni(1)−N(3)	82.42(12)	O(6)−Ni(2)−N(5)	170.12(12)
N(1)−Ni(1)−N(3)	79.21(14)	N(6)−Ni(2)−N(5)	83.77(11)

slow evaporation of the solvent, were mounted on a glass fiber, and measurements were made on a Rigaku/ADSC CCD area detector with graphite-monochromated Mo Kα; radiation (λ = 0.71073 Å). The structures were processed and corrected for Lorentz and polarization effects, and absorption using the d*TREK program.[54] The structures were solved by direct methods[55] and expanded using Fourier techniques.[56] All calculations were performed using the teXsan[57] crystallographic software package of the Molecular Structure Corporation, and SHELXL-97.[58] The non-hydrogen atoms were refined anisotropically. Hydrogen atoms were fixed in calculated positions, but not refined.

Purple needle crystals of $[GdNi_2(bcn)_2(CH_3CN)_2]ClO_4 \cdot CH_3CN$ were obtained via slow evaporation of acetonitrile. The sample was mounted on a glass fiber and cooled to 173 K. Data sets were collected on a Bruker X8 APEX CCD area detector with graphite-monochromated Mo Kα radiation (λ = 0.71073 Å). Data were collected and integrated using the Bruker SAINT[59] software package and corrected for Lorentz and polarization effects as well as for absorption (SADABS).[60] The structure was solved by direct methods (SIR92).[55] Non-hydrogen atoms were refined anisotropically, while hydrogen atoms were added but not refined. Final refinement was completed using SHELXL-97.[58] Selected crystallographic data for the complexes are presented in Tables 2 and 3 and in the Supporting Information for this paper.

Results and Discussion

Synthesis of H_3bcn. A modified Richmond−Atkins route was used to synthesize H_3bcn in higher yields than previously published[53] (Scheme 1). The phenol arms were successfully attached to the polyamine macrocycle by an *in situ* reductive alkylation with sodium triacetoxyborohydride, the only reducing agent found to prepare the desired H_3bcn in moderate to high yields, with minimal side-products.

Table 3. Selected Bond Lengths (Å) and the Intermetallic Angle (deg) in the $[GdNi_2(bcn)_2(CH_3CN)_2]ClO_4 \cdot CH_3CN$, $[YbNi_2(bcn)_2]ClO_4 \cdot CH_3CN$, and $[GdZn_2(bcn)_2(CH_3CN)_2]ClO_4 \cdot CH_3CN$ Complexes

crystal data	$GdNi_2$	$YbNi_2$	$GdZn_2$
Ln−O1	2.342(2)	2.203(6)	2.385(4)
Ln−O2	2.384(2)	2.193(6)	2.382(4)
Ln−O3	2.351(2)	2.190(7)	2.350(3)
Ln−O4	2.354(2)	2.184(6)	2.341(4)
Ln−O5	2.390(2)	2.195(6)	2.394(4)
Ln−O6	2.379(2)	2.202(6)	2.357(3)
TM1−O1	2.082(2)	2.083(6)	2.093(4)
TM1−O2	2.058(2)	2.115(6)	2.047(4)
TM1−O3	2.064(2)	2.076(6)	2.122(4)
TM2−O4	2.094(2)	2.100(6)	2.108(4)
TM2−O5	2.065(2)	2.102(6)	2.086(4)
TM2−O6	2.039(2)	2.2084(7)	2.070(4)
TM1−N1	2.083(3)	2.069(8)	2.150(5)
TM1−N2	2.069(3)	2.053(7)	2.134(4)
TM1−N3	2.074(3)	2.064(8)	2.137(4)
TM2−N4	2.068(3)	2.062(7)	2.152(4)
TM2−N5	2.079(3)	2.050(8)	2.129(4)
TM2−N6	2.067(3)	2.048(8)	2.136(4)
Ln−TM1	3.1191(5)	2.8990(13)	3.1259(7)
Ln−TM2	3.1182(5)	2.8910(13)	3.1254(6)
TM1−TM2	5.905(3)	5.787(13)	5.905(7)
TM1−Ln−TM2	142.417(13)	176.39(4)	141.68(4)

[TM(Hbcn)]·*n*H_2O Complexes. The isolation of the Ni(II)- and Zn(II)-bcn complexes was instrumental in studying the building blocks of the larger coaggregated $[LnTM_2(bcn)_2]^+$ complexes (abbreviated as $LnTM_2$). The binary transition metal complexes were synthesized using one equivalent of $TM(ClO_4)_2 \cdot 6H_2O$ (TM = Zn(II) or Ni(II)) and H_3bcn in either methanol or acetonitrile to give a parent peak with 100% relative intensity in the +ESI-MS spectra corresponding to the proton adducts of the [TM(Hbcn)] complexes.

A rigid octahedral geometry where the three phenolate oxygen donors and three amine nitrogens are tightly bound to the Zn(II) ion, is postulated from the sharp resonances observed in the ^{1}H NMR data of [Zn(Hbcn)] (Figure 2). The ring hydrogens, H3–6 are split into four distinct signals, all significantly shifted. The largest upfield shift was observed for H3, the hydrogen ortho to the chelating phenolate oxygen ($\Delta\delta \approx 0.79$ ppm). Splitting of the singlet from the benzylic protons into AB doublets upon complexation additionally confirms the rigidity of the complex. The diasterotopic hydrogens are further distinguished by assuming the proton in the pseudoaxial position, H2B, is more shielded than the benzylic proton in the pseudoequatorial environment, H2A, because of the proximity of the collinear p-orbital from the neighboring benzene ring. The excess shielding causes the pseudoaxial hydrogen to resonate at lower frequencies (3.39 vs 4.23 ppm of the pseudoequatorial proton).[61]

(54) *D*TREK Area Detector Software*,version 7.11; Molecular Structure Corporation: The Woodlands, TX, 2001.
(55) Altomare, A.; Cascarano, M.; Giaconazzo, C.; Guagliardi, A. *J. Appl. Crystallogr.* **1994**, *26*, 343.
(56) Beurskens, P. T.; Admiraal, G.; Beurskens, G.; Bosman, W. P.; de Gelder, R.; Israel, R.; Smits, J. M. M. *The DIRDIF-94 program system*; Crystallography Laboratory, University of Nijmegen: Nijmegen, The Netherlands, 1994.
(57) *teXsan: Crystal Structure Analysis Package*; Molecular Structure Corporation: The Woodlands, TX, 1985, 1992.
(58) Sheldrick, G. M. *SHELXL-97*; University of Gottingen: Germany, 1997.
(59) *SAINT*,version 6.02; Bruker AXS Inc.: Madison, WI, 1999.
(60) *SADABS*,version 2.05; Bruker AXS Inc.: Madison, WI, 1999.

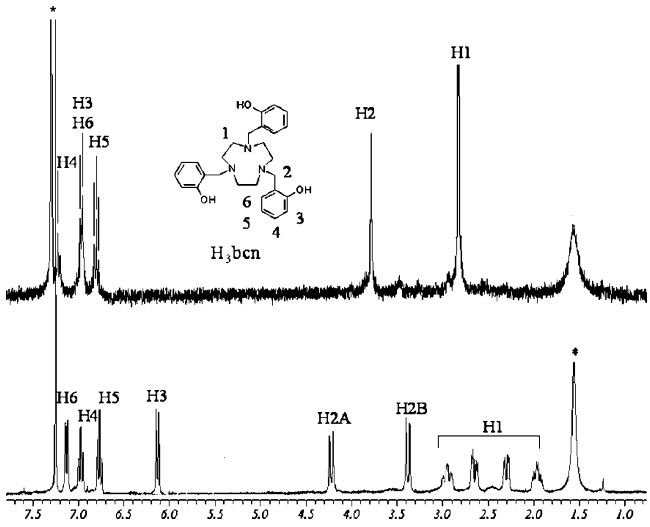

Figure 2. ^{1}H NMR spectra of H_3bcn (top) and [Zn(Hbcn)] (bottom) (300 MHz, $CDCl_3$, RT, *solvent).

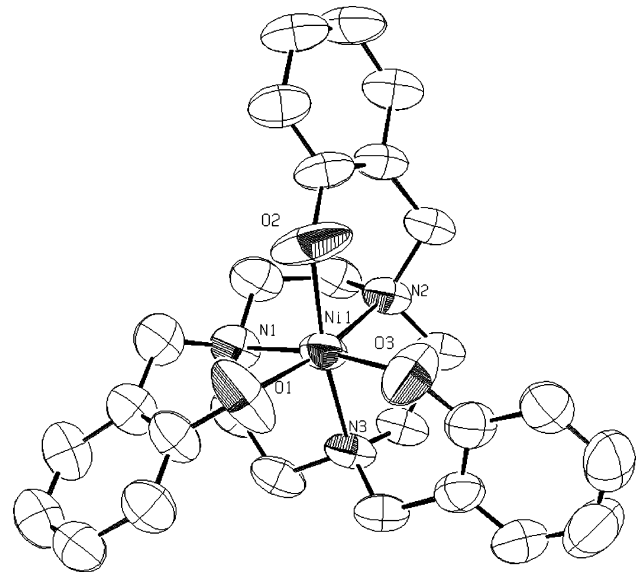

Figure 3. ORTEP diagram of the cation in $H_3[Ni(bcn)]_2(ClO_4)\cdot 3CH_3CN$; thermal ellipsoids are drawn at 50%.

In addition, the conformational constraints on the ethylenic backbone imposed by the chelation of Zn(II) renders the ethylenic hydrogens magnetically and chemically inequivalent (Figure 2) resulting in four distinct multiplets assigned to each of the ethylenic hydrogens in the $N-CH_2-CH_2-N$ bridge. Assignments were confirmed by $^1H-^1H$ COSY experiments. The elemental analysis was also consistent with a stoichiometry of $[Zn(Hbcn)]\cdot H_2O$, suggesting the formation of a neutral encapsulated product.

Interestingly, different stoichiometries of the Ni(II)−bcn complexes were isolated depending on the solvent used. A purple paramagnetic material was obtained when synthesized in acetonitrile with an EA consistent with $H_3[Ni(bcn)]_2ClO_4$, whereas a yellow diamagnetic material precipitated using the analogous reaction in methanol with the stoichiometry of $[Ni(Hbcn)]\cdot H_2O$. The purplematerial is not soluble in alcohols and only sparingly soluble in acetonitrile, whereas the yellow material is soluble in both solvents. The only difference detected in the fingerprint region of the IR is a prominent band at 1061 cm^{-1} for the purple material, correlating with a ClO_4^- counterion and confirming the formation of a cationic complex for the purple Ni(II) species. The +ESI-MS spectra for both species were nearly identical with the parent peak corresponding to the proton adduct of the [Ni(Hbcn)] complex.

The shifting of the resonances in the ^{1}H NMR spectrum, in addition to the absence of resonances corresponding to the free ligand, confirm the coordination of Ni(II) to the polyamine phenol ligand for the yellow diamagnetic species. The multiplets in the aromatic region, the broad peaks for the organic framework, and the small chemical shift changes relative to the free ligand ($\Delta\delta < 0.02$ ppm) suggest exchange of the amine nitrogens and phenol oxygens around the metal on the NMR time scale, making elucidation of the coordination sphere around the metal ion difficult. Elevating or lowering the temperature resulted in no significant sharpening, broadening, or coalescence of the resonances, implying a fluxional process in solution with a low energy barrier between interconverting states. The broadening of the hydrogen resonances may also be complicated by the exchange of the coordinated amine nitrogens and phenol oxygens with surrounding solvent molecules. The ^{1}H NMR spectrum from the paramagnetic purple Ni(II) species was uninformative.

A solid-state structure of the purple paramagnetic material $H_3[Ni(bcn)]_2ClO_4\cdot 3CH_3CN$ (Figure 3 and Table 2) revealed Ni(II) encapsulated in a distorted octahedral environment by the bcn^{3-} ligand via three phenolate O groups and three amine N functionalities. Each of the two independent Ni(II) moieties is located near an inversion center with approximate C_3 symmetry about an axis perpendicular to the plane of the bcn^{3-} ligand.

The $N_{cis}-Ni-N_{cis}$ bite angle (82.6°) about the Ni(II) center varies from the 90° idealized for an octahedral structure because of the constraints imposed by the five-membered chelate ring of the tacn moiety; however, the $N_{cis}-Ni-O_{cis}$ angle is close to 90° (89.1°), suggesting that the six-membered ring between the phenolate O and the amine N is large enough to accommodate Ni(II) in an octahedral environment (Table 2).

The average Ni−O and Ni−N bond lengths do not differ between the two $[Ni(bcn)]^-$ units (Ni(1) = 2.044 and 2.141 Å, Ni(II) = 2.031 and 2.137 Å, respectively); however, the Ni−N bonds are slightly longer than those observed for $[Ni(tacn)_2]^{2+}$ (2.139 vs 2.116 Å, respectively),[64] and significantly longer than optimum values for an octahedral NiN_6 structure of 2.08 Å.[65] The elongation of the Ni−N bonds are correlated with the less strongly coordinating tertiary

(61) Fraser, R. R.; Gurudata; Reyes-Zamora, C.; Swingle, R. B *Can. J. Chem.* **1968**, *46*, 1595.
(62) Cole, E.; Copley, R. C. B.; Howard, J. A. K.; Parker, D.; Ferguson, G.; Gallagher, J. F.; Kaitner, B.; Harrison, A.; Royle, L. *J. Chem. Soc., Dalton Trans.* **1994**, 1619.
(63) Beattle, J. K.; Elsbernd, H. S. *J. Am. Chem. Soc.* **1970**, *92*, 1946.
(64) Zompa, L. J.; Margulis, T. N. *Inorg. Chim. Acta* **1978**, *28*, L157.
(65) Graham, B.; Grannas, M. J.; Hearn, M. T. W.; Kepert, C. M.; Spiccia, L.; Skelton, B. W.; White, A. H. *Inorg. Chem.* **2000**, *39*, 1092.

nitrogens and the steric demands on the ligand upon accommodation of the Ni(II) ion, similar to that seen in a Ni_4L species, where L = tetrakis(1,4,7-triazacyclonon-1-yl).[65] Alternatively, the average Ni−O bond lengths (2.014 Å) in the $[Ni(bcn)]^-$ species are very similar to other deprotonated phenoxide species.[22,41] It is also interesting to note that the Ni−N and Ni−O distances in the axial positions are slighter longer than the comparable bonds in the equatorial positions (2.050 and 2.136 Å vs 2.021 and 2.132 Å, respectively) attributed to steric strain of the ligand.

Three bridging hydrogens equidistant to the six phenolic oxygen atoms were found between the two encapsulated Ni(II) structures. The dimers have intermolecular O−O contacts (2.705 Å) consistent with other O−HO hydrogen bonds in the literature (near 2.8 Å); however, the exact location of the O−H hydrogen atoms could not be located because of the three hydrogens being disordered over the six possible sites. The large thermal ellipsoids on the oxygens, expected for intermolecular hydrogen bonding, suggest that the hydrogen atoms reside between the two halves of the molecule rather than being bound to one-half of the complex. One perchlorate and three noncoordinating acetonitrile molecules were also found in the unit cell.

On the basis of the diamagnetic properties, it is postulated that the yellow [Ni(Hbcn)] material is a square planar d^8 Ni(II); this hypothesis is strengthened by analyzing the UV–vis data of the yellow material. One weak band resolved at 586 nm, resulting from the $^1A_{1g} \rightarrow {}^1A_{2g}$ transition, matches literature values for Ni(II) in the square planar conformation.[49,66] The purple Ni(II) complex has absorbances characteristic for an octahedral environment, arising at 544 and 900 nm from $^3A_{2g}(F) \rightarrow {}^3T_{1g}(F)$ and $^3A_{2g}(F) \rightarrow {}^3T_{2g}(F)$ transitions, respectively.[36,41]

It is also interesting to note that the yellow material can readily be converted to the purple material by dissolution and refluxing in a variety of solvents, including acetonitrile. The purple material, however, could not be converted into the yellow diamagnetic material indicating that the yellow complex is an intermediate. This point is confirmed by allowing a sample of the yellow Ni(II) material to stand in methanol for several weeks. During this time, the solution turns red and purple crystals deposit that solve for the same stoichiometry as the purple paramagnetic Ni(II) complex.

$[TM_3(bcn)_2]\cdot nH_2O$ Complexes. Addition of 1 equiv of $TM(ClO_4)_2\cdot 6H_2O$ to 2 equiv of deprotonated $[TM(bcn)]^-$ formed trimetallic transition metal species with the expected stoichiometry confirmed by EA ($[Ni_3(bcn)_2]\cdot 2H_2O$ for the trimetallic Ni(II) species and $[Zn_3(bcn)_2]$ for the trimetallic Zn(II) complex). The peaks in the +ESI-MS spectra that correlate to the trimetallic species (with the expected isotope patterns) only resolved for 10% of the relative intensity, suggesting that the stability of the neutral $[TM_3(bcn)_2]$ complexes was significantly reduced compared to that of the respective [TM(Hbcn)] building block species (the parent peak with 100% relative intensity corresponded to the proton adduct of the monometallic [TM(Hbcn)] complexes). The only differences observed in the IR of the monometallic and the trimetallic TM(II) species was the bathochromic shift of the υ_{C-O} bands attributed to decreased strength in the phenolate oxygen O−TM dative bond from the oxygens bridging an additional metal.

Only one set of resonances is seen in the ^1H NMR spectra for $[Zn_3(bcn)_2]$, implying a 3-fold symmetric complex where the Zn(II) is held in a rigid octahedral geometry. A small upfield shift of the hydrogen (H3) ortho to the phenolate oxygen ($\Delta\delta \approx 0.01$) compared to the [Zn(Hbcn)] spectra was observed. Slight upfield shifts and larger couplings between the protons on the ethylenic bridge are also observed suggesting an increasingly strained environment upon bridging the third Zn(II) metal ion ($\Delta\delta \approx 0.11$ ppm, $\Delta^3J \approx 1.2$ Hz, $\Delta^2J \approx 0.8$ Hz for H1).

$[LnTM_2(bcn)_2]ClO_4\cdot nH_2O$. Air-stable complexes of the trinuclear $[LnTM_2(bcn)_2]ClO_4\cdot nH_2O$ unit were produced using protocols adopted from the synthesis of analogous $[LnNi_2(tam)_2]^+$ and $[LnNi_2(trn)_2]^+$ cationic species (TM = Ni(II) and Zn(II), Ln = La(III), Nd(III), Gd(III), Dy(III), Yb(III)).[36,41] Spontaneous, self-assembled bicapped structures, where the Ln(III) is bridged between the three deprotonated phenolate oxygens from two $[TM(bcn)]^-$ preorganized ligands, were readily formed. The amount of base added is instrumental to the formation of these complexes; the desired d/f/d complexes were not isolated if a slight excess or shortage of the base was used. The complexes precipitated from the respective reaction mixtures affording light-purple or off-white solids for the Ni(II)− or Zn(II)−Ln(III) species, respectively (Scheme 2).

Attempts to recrystallize the complexes (in hot MeOH/H_2O or CH_3CN/H_2O) or purification by column chromatography resulted in decomposition of the product and presumed hydrolysis of the Ln(III) ions. Washing the precipitated solid thoroughly with cold solvents to remove unreacted ligand, additional $Ln(ClO_4)_3$ and $TM(ClO_4)_2$ salts, or other side products, was the only way to yield complexes pure by elemental analysis (if the trimetallic d/f/d species did not crystallize upon standing in solution). The compounds were characterized by EA, +ESI-MS, IR, and NMR (only of the diamagnetic $[LaZn_2(bcn)_2]^+$). All results are consistent with the formation of cationic d/f/d species shown in Table 1. The elemental analyses for all the lanthanide complexes agreed with the empirical formula $[LnTM_2(bcn)_2]ClO_4\cdot nH_2O$ suggesting that labile reaction solvent molecules (either acetonitrile of methanol) observed in the solid state crystal structure analysis were replaced with water molecules upon storage under air. Hydrated species have been observed with previously synthesized Ln(III)-containing systems where coordinated solvent molecules are associated with the metal to fulfill the large coordination preference of the Ln(III) ions.

Electrospray ionization mass spectrometry in the positive ion mode was the primary diagnostic tool for the detection of the cationic d/f/d clusters, giving diagnostic mass spectra with the expected isotopic patterns. The mass spectra are devoid of any other significant peaks besides the parent ion

(66) Lever, A. B. P. *Inorganic Electronic Spectroscopy*; Elsevier: New York, 1984.

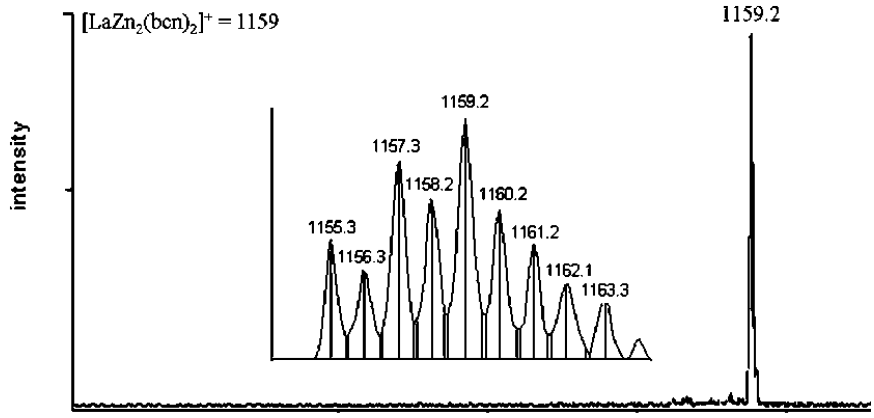

Figure 4. +ESI spectrum of $[LaZn_2(bcn)_2]^+$; inset displays the experimental isotope pattern closely matching the calculated.

peak for the cationic complex, $[LnTM_2(bcn)_2]^+$ (Figure 4). The isotope patterns were also in good agreement with the calculated patterns.

The two TM(II) in the $[LnTM_2(bcn)_2]^+$ cationic complexes appear to be in comparable coordination environments in solution, as reflected by the absence of splitting of the absorbance peaks in the UV–vis. The absorptions at 900 and 544 nm for the octahedral Ni(II) are associated with $^3A_{2g}(F) \rightarrow {}^3T_{2g}(F)$ and $^3A_{2g}(F) \rightarrow {}^3T_{1g}(F)$ transitions, respectively.[36,41] The $^3A_{2g}(F) \rightarrow {}^3T_{1g}(P)$ transition is obscured by a strong charge-transfer band at 303 nm. A $\pi-\pi^*$ transition of the K-band of the benzene ring appears at 249 nm.[42] The spectrum of the d/f/d species is very similar to that of the octahedral [Ni(Hbcn)] system, suggesting that the incorporation of the Ln(III) does not significantly distort the coordination environment around the Ni(II) ion.

The ^{1}H NMR spectrum was instrumental in elucidating the solution structure of the $[LaZn_2(bcn)_2]^+$ complex. The relative shifts in the resonances conclusively indicate binding of the ligand to the metal ions. Interestingly, the ^{1}H NMR spectrum of $[LaZn_2(bcn)_2]^+$ is nearly superimposable upon that of [Zn(Hbcn)], suggesting that the TM(HL) structure is maintained upon coordination to the La(III) ion. The minor differences observed between the two spectra include the ring proton resonances being shifted slightly upfield upon accommodating the Ln(III) ion ($\Delta\delta \approx 0.02$ ppm) compared to those in the ^{1}H NMR spectra for [Zn(Hbcn)]. The ethylenic and benzylic proton resonances (which exhibit the same splitting seen for the [Zn(Hbcn)] and $[Zn_3(bcn)_2]$ species) are also slightly shifted upfield from the Zn(II) complexes ($\Delta\delta > 0.03$ ppm) possibly because of the smaller donation of electron density to La(III). The absence of additional splitting of the resonances further suggests that the 3-fold symmetry is maintained. In addition, only one set of resonances in the ^{13}C NMR spectrum was observed; one peak for each of the carbons in the ring, one resonance for the benzylic carbon and one peak for the chemically and magnetically equivalent carbons in the ethylenic bridge.

Regardless of the TM(II) or the Ln(III) used, the IR spectra for the $[LnTM_2(bcn)_2]ClO_4 \cdot nH_2O$ complexes were nearly superimposable in the 400–3500 cm^{-1} range, suggesting the formation of isostructural complexes in the solid state. The small <10 cm^{-1} variations in the IR peak frequencies between Ln(III) ions and Ni(II) or Zn(II) are attributed to mass differences among the metal ions. The small differences between the TM/Ln complexes were also confirmed by the crystal structure of $[GdNi_2(bcn)_2(CH_3CN)_2]ClO_4 \cdot CH_3CN$ and the analogous $[GdZn_2(bcn)_2(CH_3CN)_2]ClO_4 \cdot CH_3CN$.

Both the $[GdNi_2(bcn)_2]^+$ and $[GdZn_2(bcn)_2]^+$ cations of the perchlorate salt (Figure 5, Table 3) revealed a V-shaped metallic core where the Zn(1)−Gd−Zn(2) angle is slightly smaller (141.68°) than that observed for the Ni(1)−Ln−Ni(2) complexes (142.4°). The Gd(III) ion is eight-coordinate in a square antiprism distorted to C_{2v} bicapped trigonal prism[36,67] geometry, bicapped by two deprotonated tridentate $[Ni(bcn)]^-$ or two $[Zn(bcn)]^-$ units, plus two coordinating acetonitrile molecules. The end capping units are nearly identical with each TM(II) chelated in a distorted octahedral geometry via the three amine and three phenolato functions from the fully deprotonated bcn^{3-} ligand, similar to the coordination mode seen for the paramagnetic $H_3[Ni(bcn)]_2ClO_4 \cdot 3CH_3CN$ species. The Ni−N and Ni−O bond distances in $[GdNi_2(bcn)_2(CH_3CN)_2]ClO_4 \cdot CH_3CN$ are slightly longer than those observed in $H_3[Ni(bcn)]_2ClO_4 \cdot 3CH_3CN$ but very similar to other literature d/f complexes. In addition, the TM−O, TM−N, and Gd−O bond lengths in the trimetallic species are nearly identical regardless of the TM(II). The averaged Zn−Gd distance is slightly longer (3.125 Å) than the Ni−Gd distance of 3.119 Å attributed to the larger ionic radius of the Zn(II) ion; however, the interatomic Zn−Zn distance is nearly identical with the Ni−Ni distance in the TM−Ln−TM complexes (5.905 Å).

A decrease in the number of coordinated solvent molecules surrounding the smaller Ln(III) ions is observed for $[YbNi_2(bcn)_2]ClO_4 \cdot CH_3CN$, where the Yb(III) is 6-coordinated by six bridging phenolate oxygens. The decrease of the coordination number with the increasing atomic number, that is, decrease in ionic radius, is commonly observed for Ln(III) systems, especially in systems containing labile coordinated solvent molecules. All Ln−O bond lengths uniformly reflect the periodic decrease in the ionic radius of the Ln(III) ion (2.367 Å for Gd(III) and 2.177 Å for Yb(III)), as well as the compressed O−Yb−O angle (average of 77.6°)

(67) Muetterties, E. L.; Guggenberger, L. J. *J. Am. Chem. Soc.* **1974**, *96*, 1748.

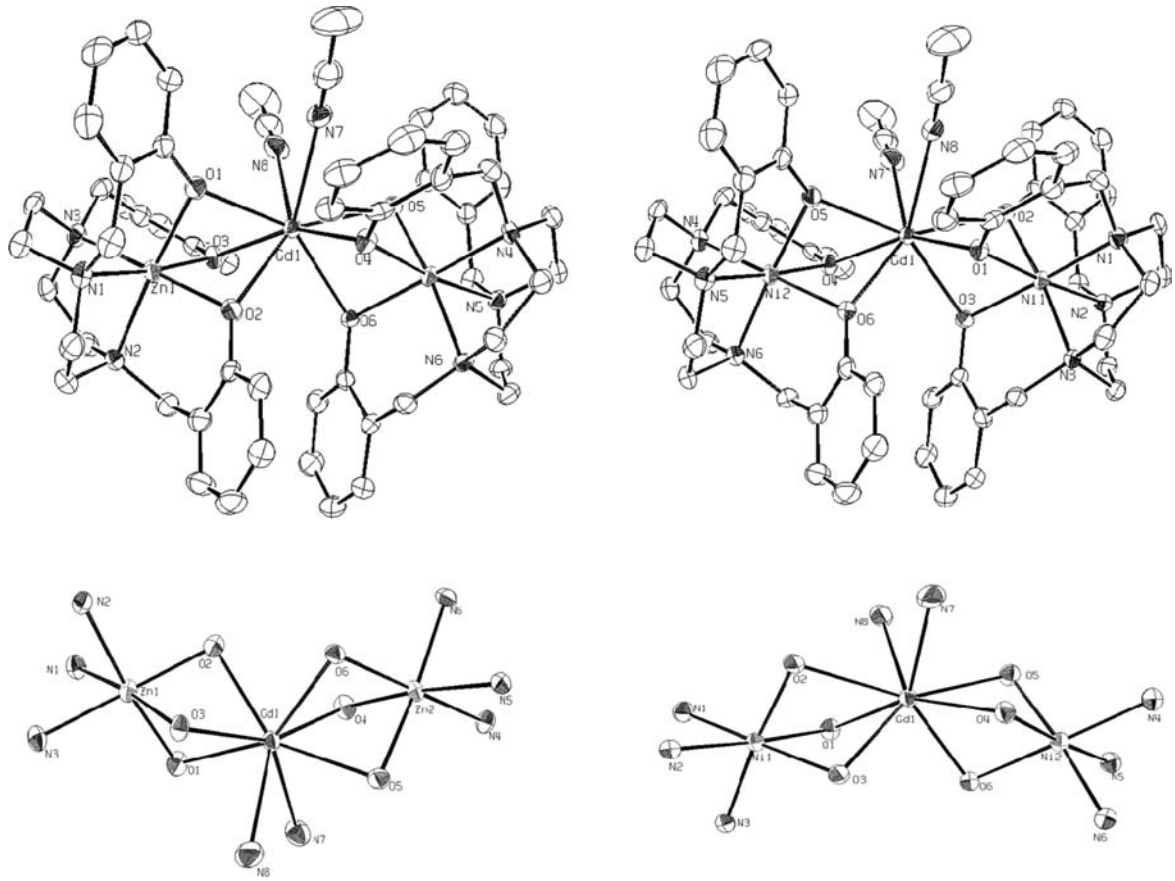

Figure 5. ORTEP diagrams of the cations in $[GdNi_2(bcn)_2(CH_3CN)_2]ClO_4$ (right) and $[GdZn_2(bcn)_2(CH_3CN)_2]ClO_4$ (left) with expanded views of the Gd(III) coordination sphere; thermal ellipsoids are drawn at 50% probability.

compared to 84.6° for the Gd(III) complex. The Ni−Yb−Ni angle displays a nearly linear metallic core of 176.4°. The intermetallic bonds for Ni−Yb are slightly shorter than the Ni−Gd bonds (2.895 vs 3.119 Å), with a Ni−Ni interatomic distance of 5.787 Å. Uniquely, these d/f/d complexes do not contain coordinated counterions. Powder diffraction data was also collected for the $GdNi_2$ and $YbNi_2$ systems; however, the data did not match the crystal data because of differences in solvation. Upon standing in air, these compounds are known to exchange coordinated reaction solvents (methanol or acetonitrile) for ambient water observed both in the IR and EA spectra, and assumed to be the cause of the differences in the powder and crystal diffraction data.

Magnetic Properties. The magnetic susceptibilities of the $[LnTM_2(bcn)_2]ClO_4 \cdot nH_2O$ species were collected on powdered samples using a SQUID magnetometer over a temperature range of 2−300 K. Unfortunately, regression values at high temperatures (>100 K) are only adequate for data taken at the higher magnetic field (10 000 G). Thus, all $\chi_M T$ values reported at RT will be those measured at a magnetic field of 10 000 G. To minimize effects from magnetic saturation, $\chi_M T$ values reported herein at <100 K were those obtained using the magnetic field of 500 G. All measurements were corrected for diamagnetism using Pascal's constants.[51]

The free-ion approximation, where only one level $^{2S+1}L_J$ is thermally populated and second-order contributions are ignored, is a good approximation of the magnetic susceptibility, χ_M, at room temperature (RT) for many rare earth compounds. Thus, the experimental data will be compared to the calculated values derived from eq 1

$$\chi_M T = [2 \times g_{Ni}{}^2 S_{Ni}(S_{Ni}+1) + g_J{}^2 J(J+1)]/8 \qquad (1)$$

where g is the Landé factor fixed at 2.00, $g_J = 3/2 + [S(S+1) - L(L+1)](2J(J+1))^{-1}$, L is the total orbital angular moment quantum number, S is the total spin angular moment quantum number, and J is the total angular momentum quantum number.

The RT $\chi_M T$ values for $[LnZn_2(bcn)_2]ClO_4 \cdot nH_2O$, where Ln = Nd(III), Gd(III), Dy(III), and Yb(III), were determined to be $\chi_M T$ = 1.67, 7.56, 14.16, and 1.95 cm^3 K mol^{-1}, respectively, shown in Figure 6. These values closely correspond to the calculated RT values (1.69, 7.88, 14.13, and 2.57 cm^3 K mol^{-1} using eq 1) where the magnetic contribution is solely originating from the isolated Ln(III) ion. The $\chi_M T$ decreases slightly as the temperature is lowered from 300 to 10 K for all $LnZn_2$ species. Below 10 K, the $\chi_M T$ decreases significantly reaching a minimum at 2 K, an intrinsic characteristic of Ln(III) attributed to the depopulation of the spin–orbit sublevels similar to that seen in other d/f and d/f/d heterometallic species.[31,36,41,48]

The absence of a magnetic exchange between the d/f/d metals for the $LnZn_2$ systems make these species an attractive baseline for the analogous paramagnetic Ni(II) systems, similar to the empirical approach developed by Costes et

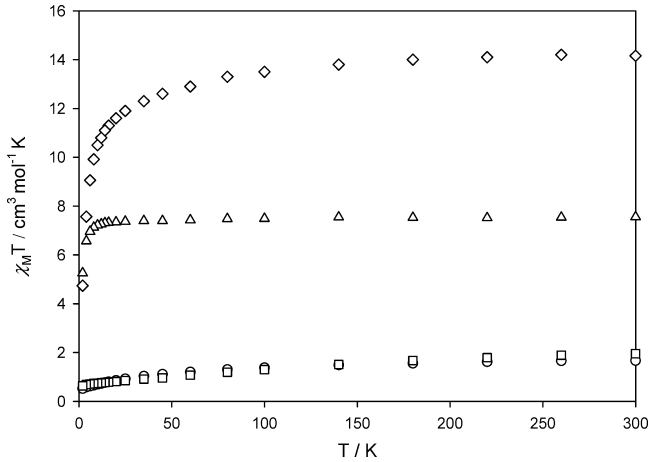

Figure 6. Temperature dependence of $\chi_M T$ for $[LnZn_2(bcn)_2]ClO_4 \cdot nH_2O$ complexes at 10 000 G: (○) $NdZn_2$; (△) $GdZn_2$; (◇) $DyZn_2$; (□) $YbZn_2$.

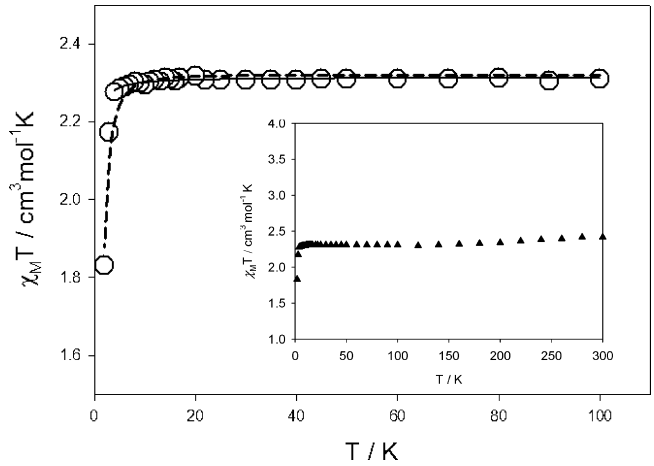

Figure 7. $\chi_M T$ vs T plot of $[LaNi_2(bcn)_2]ClO_4 \cdot 3H_2O$ at 500 G from 100−2 K (○) or at 10 000 G from 300−2 K (insert, ▲). The solid and the dotted lines represent the theoretical curve (text) fit from 100 to 4 K or 100 to 2 K, respectively.

al.[31] and used by Kahn,[32,44] Ōkawa,[45,48] and Matsumoto[35] and co-workers. Costes et al. removed the unquenched orbital angular momentum contributions from the Ln(III) by calculating the difference, $\Delta(\chi_M T)$, between the $\chi_M T$ values for the Cu−Ln species and the structurally homogeneous Ni−Ln complexes, where the diamagnetic Ni(II) was held in a square planar geometry. The magnetic exchange between the d/f/d metal ions for the complexes herein were elucidated using a similar empirical approach defined by eq 2.

$$\Delta\chi_M T = (\chi_M T)_{LnNi_2} - (\chi_M T)_{LnZn_2} = 2(\chi_M T)_{Ni} + J_{NiLn}(T) \quad (2)$$

Ln = La(III), Nd(III), Gd(III), Dy(III), and Yb(III) and $J_{NiLn}(T)$ is related to the nature of the overall exchange interaction between the Ni(II) and Ln(III), such that positive or negative values indicate a ferromagnetic or antiferromagnetic interaction, respectively. Similar crystal field effects are assumed to be operative in both the Ni(II) and Zn(II) complexes due to similarities in their core structures. Intermolecular Ni(II)−Ni(II) magnetic interactions are assumed to be negligible for the d/f/d systems.

The $\chi_M T$ plot of $[LaNi_2(bcn)_2]ClO_4 \cdot 3H_2O$ corresponds well to the expected curve for isolated Ni(II) ions (Figure 7). $LaNi_2$ exhibits a $\chi_M T$ value of 2.42 cm^3 mol^{-1} K at RT, corresponding to two Ni(II) ions with μ_{eff} per Ni(II) = $3.11\mu_\beta$ and $g = 2.10$. Below 10 K, the $\chi_M T$ curve for $LaNi_2$ decreases rapidly due to zero-field splitting of the octahedral Ni(II) transition metal ion or weak intra and/or intermolecular antiferromagnetic interactions, also seen in $[LaNi_2(tam)_2]^+$ and $[LaNi_2(trn)_2]^+$. Nonetheless, the μ_{eff} values determined for the two Ni(II) ions are in the range of previously reported literature values.[68]

In order to confirm the extent of interaction between the two terminal Ni(II) ions, we examined fits of the $LaNi_2$ data to the theoretical model described by Shiga et al.[45] Attempts to fit the data to this model over the full 2−100 K temperature range were unsuccessful unless the 2 and 3 K data were ignored. Attempts to fit the data over the 4−100 K range employing g_{Ni}, the exchange parameter J' and temperature independent paramagnetism, TIP, as variable parameters, invariably gave vanishingly small values for TIP. Accordingly, we set TIP to zero and employed g_{Ni} and J' as variable parameters to get the best fit shown as the solid line in Figure 7. The best fit gave $g_{Ni} = 2.151$ (0.0001), $J' = -0.030$ cm^{-1} (0.003), and $F = 1.63 \times 10^{-5}$. F is the goodness of fit value given by eq 3 where N is the number of data points.

$$F = [1/N[\Sigma(\chi_{calc}) - (\chi_{obsd})^2/\Sigma(\chi_{obsd})^2]]^{1/2} \quad (3)$$

Our inability to fit the lowest temperature data to the model likely arises from the fact that the strong temperature dependence of χT in this region arises primarily from the effects of zero field splitting of Ni(II), an effect not included in this model. This analysis, which avoids this region, can be considered to give a valid measure of the strength of the interaction between the Ni centers and the clear conclusion from this is that the coupling is extremely small. The J' value of −0.03 cm^{-1} is, for example, 20 times smaller than that observed by Shiga et al. for their Ni−La−Ni compound ($J = -0.63$ cm^{-1}).[45] This result prompted us to attempt to fit our data to a ZFS model[69] in which exchange coupling is ignored. Setting $J' = 0$ and TIP = 0, as above, and employing g_{Ni} and D, the ZFS parameter, as variable parameters, the best fit to the data over the full range from 2−100 K is shown as the dotted line in Figure 7. This fit yielded $g = 2.154$ (0.003), $D = 2.60$ (0.07), and $F = 6.52 \times 10^{-4}$. The goodness of this fit confirms that the abrupt drop observed in $\chi_M T$ at the lowest temperatures is due primarily to ZFS and that the exchange coupling between the nickel centers (ignored in this particular model) is very weak in this compound.

The $\chi_M T$ value for the $[LnNi_2(bcn)_2]ClO_4 \cdot nH_2O$ species followed the isolated-ion approximation of three isolated metal ions at RT. The $\chi_M T$ for $NdNi_2$ was determined to be 3.70 cm^3 K mol^{-1} at RT, closely matching the value (3.64 cm^3 K mol^{-1} calculated using eq 1) expected for two magnetically isolated Ni(II) ions ($S_{Ni} = 1$) and one Nd(III)

(68) Earnshaw, A. *Introduction to Magnetochemistry*; Academic Press: New York, 1968.

(69) O'Connor, C. J. *In Progress in Inorganic Chemistry*; Lippard, S. J., Ed.; Interscience: New York, 1982; Vol. *29*, pp 203.

Table 4. Observed and Calculated Magnetic Susceptibilities for $[LnNi_2(bcn)_2]ClO_4 \cdot nH_2O$ Complexes

Ln(III)	ground state	g_J	$\chi_M T^a$ (calcd)	$\chi_M T_{obsd}$ (RT)	$\chi_M T_{obsd}$ (2 K)	$\chi_M T_{max\ or\ min}$ (T K)	$\Delta(\chi_M T)^b$	sign of $J_{NiLn}(T)^c$
La	$^1S_0$		2.85	2.00	2.55	2.55 (2)		
Nd	$^4I_{9/2}$	8/11	3.64	3.70	1.02	1.02 (2)	0.44	−
Gd	$^8S_{7/2}$	2	9.88	10.80	16.06	17.55 (13)	8.86	+
Dy	$^6H_{15/2}$	4/3	16.17	17.48	14.73	14.85 (3)	6.08	+
Yb	$^2S_{7/2}$	8/7	4.57	5.05	4.26	4.26 (2)	3.56	+

[a] $\chi_M T$ calculated using eq 1. [b] $\Delta(\chi_M T)$ values were obtained using eq 2 at 2 K. [c] The sign of $J_{NiLn}(T)$ was determined after removing both Ln(III) and Ni(II) contributions (eq 5).

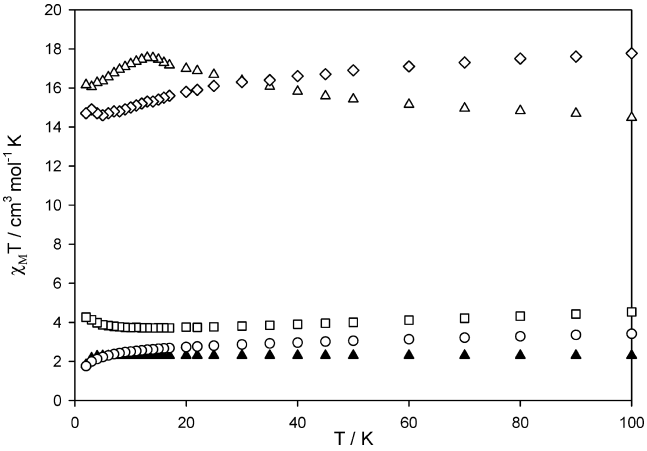

Figure 8. Temperature dependence of $\chi_M T$ for $[LnNi_2(bcn)_2]ClO_4 \cdot nH_2O$ complexes at 500 G: (▲) $LaNi_2$; (○) $NdNi_2$; (△) $GdNi_2$; (◇) $DyNi_2$; (□) $YbNi_2$.

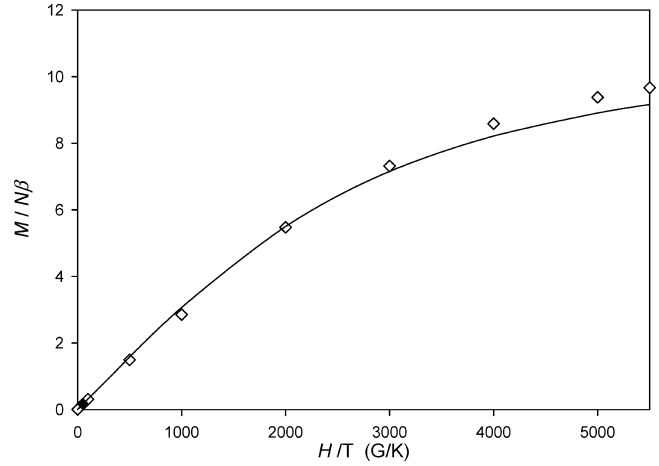

Figure 9. M vs H curve for $[GdNi_2(bcn)_2]ClO_4 \cdot H_2O$ at 10 K. The solid line indicates the theoretical curve for $S_t = 11/2$ ($g = 2$).

ion ($J = 9/2$, $g_J = 8/11$, Table 4, Figure 8). As the temperature decreased, the $\chi_M T$ values reached a minimum of 1.02 cm^3 K mol^{-1} at 2 K, well below the calculated value of 3.64 cm^3 K mol^{-1}.

The $\chi_M T$values at RT for $[GdNi_2(bcn)_2]ClO_4 \cdot H_2O$, $[DyNi_2(bcn)_2]ClO_4 \cdot H_2O$, and $[YbNi_2(bcn)_2]ClO_4$ were determined to be 10.80, 17.48, and 5.05 cm^3 K mol^{-1}, respectively, closely matching the calculated values (9.88, 16.17, and 4.57 cm^3 K mol^{-1}, respectively, using eq 1 and Table 4) for three magnetically isolated metal ions. The $\chi_M T$ data for $GdNi_2$ rise subtly reaching a maximum of 17.55 cm^3 K mol^{-1} at 13 K and decrease slightly to reach a value of 16.06 cm^3 K mol^{-1} at 3 K (Figure 8). Although the absolute reason for the observed maximum at 13 K is not known, one reviewer suggested it may be due to intermolecular antiferromagnetic interactions (further observed in the modeling of the $\chi_M T$ curve as discussed below) caused by dipolar effects. The maximum value at 13 K is significantly greater than the calculated value for the three isolated metal ions of 9.88 cm^3 K mol^{-1} and closely matches the $\chi_M T$ for a ferromagnetic coupling of the spins ($\chi_M T = 17.88$ μ_B) calculated using eq 4.

$$\chi_M T = (g[S_T(S_T + 1)])^{1/2}/2.828)^2 \qquad (4)$$

$S_T = 2S_{Ni} + S_{Ln}$ ($S_{Ni} = 1$, $S_{Gd} = 7/2$ for $[GdNi_2(bcn)_2]ClO_4 \cdot H_2O$), and g is the Landé factor ($g = 2$).

In addition, the M vs H curve follows the Brillouin function for a $S_T = 11/2$ ($S_{Ni} = 1$ and $S_{Gd} = 7/2$), suggesting that the ground state ($S_T = 11/2$), arising from a ferromagnetic interaction, is significantly populated at 10 K (Figure 9). The $[GdNi_2(bcn)_2]ClO_4 \cdot H_2O$ system follows the trend of other Ni−Gd systems reported where a ferromagnetic exchange was determined between the Ni(II) and Gd(III) metal ions.

We examined fits of the magnetic data for $GdNi_2$ to the model described by Shiga et al.[45] in which exchange integrals J, between Ni(II) and Gd(III) centers, and J', between Ni(II) centers, are considered. To minimize the number of potential variables, we examined fits where g_{Gd} was fixed at 2.00, g_{Ni} was fixed at 2.15, the value determined by analysis above of the $LaNi_2$ data, and TIP was fixed at 0.000 320 cm^3 mol^{-1}, the same value of TIP used in the data analysis by Shiga et al.[45] Fixing J' at −0.03 cm^{-1}, the value determined above for the exchange between Ni(II) centers in $LaNi_2$ complex, and allowing only J to vary, did not lead to acceptable fits. To illustrate this, we have shown the best "fit" which was obtained for $J = 4.5$ (0.6) cm^{-1} as the solid black line in Figure 10. Allowing for intermolecular coupling by incorporating a θ term (as T−θ) in the theoretical expression, we were able to reproduce the maximum in $\chi_M T$ near 13 K as seen by the dotted black line in Figure 10. This curve, which is still a very poor fit to the data, was the best fit obtained where J and θ were allowed to vary. The values of J and θ for this fit are 5.15 (0.3) cm^{-1} and −0.63 (0.07) K, respectively.

Better modeling of the data for the $GdNi_2$ complex was obtained when we allowed both J and J' to vary, as well as θ. This modeling gave the best fit curve shown as the red dotted line in the Figure 10 with $J = 11.0$ (1) cm^{-1}, $J' = -16$ (2) cm^{-1}, $\theta = -0.49$ (0.04) K, and $F = 3.8 \times 10^{-3}$. While the theoretical curve closely models the data above the maximum, the detail below the maximum is poorly modeled. Setting θ to zero and fitting only the data above the maximum (13−100 K) yielded the solid red line shown

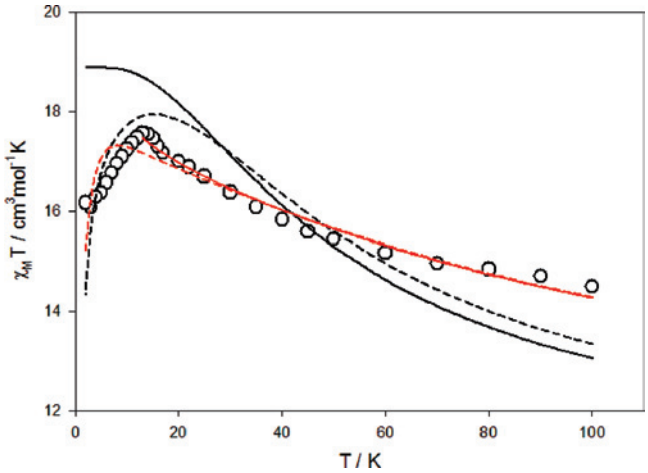

Figure 10. Attempted fittings (text) of the $\chi_M T$ vs T data for the $[GdNi_2(bcn)_2]ClO_4 \cdot H_2O$ complex (○).

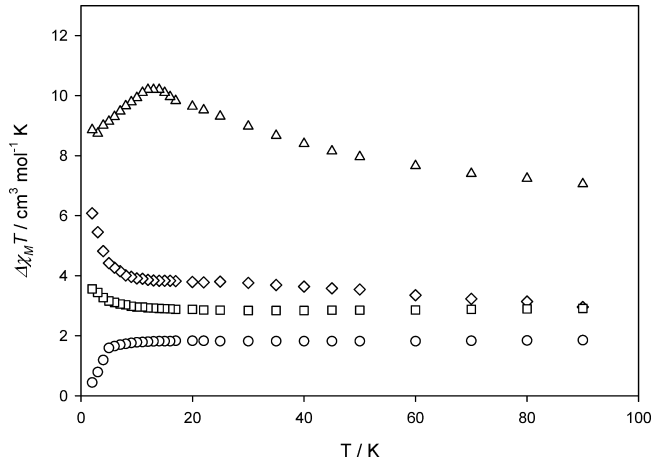

Figure 11. $\Delta\chi_M T$ for $[LnNi_2(bcn)_2]ClO_4 \cdot nH_2O$ complexes: (○) $NdNi_2$; (△) $GdNi_2$; (◇) $DyNi_2$; (□) $YbNi_2$.

in Figure 10 for which $J = 11.0$ (0.4) cm^{-1}, $J' = -17$ (1) cm^{-1}, and $F = 4.3 \times 10^{-4}$. Importantly, both of these analyses yield large positive values of J(11 cm^{-1}) confirming the presence of a relatively strong ferromagnetic exchange between the Ni(II) and Gd(III) centers much larger than previously observed. For comparison, Shiga et al. observed $J = 0.79$ cm^{-1} for their system.[45] More surprisingly, perhaps, is the large negative value of J' obtained from the fits ($J' = -16$ to -17 cm^{-1}).

In view of the difficulties encountered here in analyzing the data for the $GdNi_2$ complex and in obtaining satisfactory experimental data at temperatures above 100 K, caution should be applied in interpreting these results; particularly the numerical values presented. Nonetheless the results do point to some interesting general conclusions. There is clearly evidence for significant ferromagnetic coupling between the Gd(III) and Ni(II) centers. Moreover, it seems difficult to ignore the significant antiferromagnetic exchange seen, likely between the two Ni(II) centers. In view of the fact that the La(III) analogue studied here clearly gives no evidence for significant coupling between the Ni(II) centers, this latter finding suggests that it is not reasonable to always assume that coupling between two d-metal centers separated by an f-metal is necessarily unaffected by what metal occupies the central site. Furthermore, the presence of measurable antiferromagnetic Ni−Ni interactions in combination with significant ferromagnetic Ni−Gd coupling in such a Ni−Gd−Ni system would represent a unique form of spin-frustration. Future studies on this and related Ni/Gd systems are clearly warranted by this work.

The curve for $[DyNi_2(bcn)_2]ClO_4 \cdot H_2O$ decreases slightly until 30 K where $\chi_M T$ begins to decrease reaching a minimum value of 14.55 cm^3 K mol^{-1} at 5 K and a maximum value of 14.85 cm^3 K mol^{-1} at 3 K (Table 4). A maximum $\chi_M T$ value of 4.26 cm^3 K mol^{-1} at 2 K is determined for $[YbNi_2(bcn)_2]ClO_4$. The $\chi_M T$ values for $DyNi_2$ and $YbNi_2$ (14.85 cm^3 K mol^{-1} at 3 K; 4.26 cm^3 K mol^{-1} at 2 K, respectively) are below the calculated values of 16.17 cm^3 K mol^{-1} and 4.57 cm^3 K mol^{-1}, respectively, for two Ni(II) ions and the Dy(III) or the Yb(III) ions.

The differences between the $\chi_M T$ plots of $[LnNi_2(bcn)_2]ClO_4 \cdot nH_2O$ and the analogous $[LnZn_2(bcn)_2]ClO_4 \cdot nH_2O$ species are shown in Figure 11. Compounds $LnNi_2$, where Ln = Gd(III), Dy(III), Yb(III) displayed $\Delta(\chi_M T)$ values between 2 and 3 cm^3 K mol^{-1} at 300 K which correspond to the magnetic contributions of the two isolated Ni(II) ions. Values of 8.86, 6.08, and 3.56 cm^3 K mol^{-1} were observed, respectively, after removing the first-order orbital contributions of the Ln(III) at 2 K. These values are all larger than $\chi_M T = 2$ cm^3 K mol^{-1} calculated for two Ni(II) ions ($g = 2.0$), suggesting a ferromagnetic exchange. Alternatively, after removing the Nd(III) contributions, $NdNi_2$ shows a minimum $\Delta(\chi_M T)$ value of 0.441 cm^3 K mol^{-1}, significantly smaller than the contribution from two isolated Ni(II) ions at 2 K ($\chi_M T = 2$ cm^3 K mol^{-1}) confirming an antiferromagnetic interaction between the TM(II) and Ln(III) ions.

Furthermore, the Ni(II) contribution can be removed by using the analogous $[LaNi_2(bcn)_2]ClO_4 \cdot 3H_2O$ magnetic data to minimize any second-order effects of the Ni(II) ion that may complicate the analysis of the magnetic exchange using eq 5.

$$J_{NiLn}(T) = (\chi_M T)_{LnNi_2} - (\chi_M T)_{LnZn_2} - (\chi_M T)_{LaNi_2} \qquad (5)$$

This empirical approach helps confirm the type of spin interaction between the d/f/d metal ions, leaving only the temperature dependent $J_{NiLn}(T)$ value where a negative value suggests an antiferromagnetic exchange between metal ions and a positive value suggests a ferromagnetic exchange. Positive $J_{NiLn}(T)$ values were observed after removing Ni(II) contributions from the $\Delta(\chi_M T)$ plot at 2 K for Gd(III), Dy(III), and Yb(III) ions (5.70, 2.93, and 0.406 cm^3 K mol^{-1}, respectively), further confirming a ferromagnetic exchange. Alternatively, $NdNi_2$ has a negative $J_{NiLn}(T)$ value at 2 K of -2.72 cm^3 K mol^{-1}, further suggesting an antiferromagnetic interaction; however, we would like to note that the concluding magnetic exchanges of the $YbNi_2$ and $NdNi_2$ complexes are assigned with caution due to the slight increase or decrease of the $\Delta(\chi_M T)$ plots at low temperatures.

Only four other trimetallic $LnNi_2$ systems have been reported;[45] two of the systems were previously synthesized in our group,[36,41] and only the Ni−Gd−Ni species of the other trimetallic $LnNi_2$ complexes were analyzed.[37] The magnetic data for the $[LnNi_2(bcn)_2]ClO_4 \cdot nH_2O$ complexes matched Ōkawa and co-workers $LnNi_2$ system[45] and that of Bayly et al.[41] where a ferromagnetic exchange was observed when Ln = Gd(III), Dy(III), and Yb(III) and an antiferromagnetic interaction when Ln = Nd(III); however, this data conflicts with the antiferromagnetic interaction determined for similar amine phenol $[LnNi_2(tam)_2]ClO_4 \cdot nH_2O$ species, where Ln = Dy(III) or Yb(III).[36]

It has been proposed[41] that the observation of the antiferromagnetic interactions in the $[LnNi_2(tam)_2]ClO_4 \cdot nH_2O$ species were due to a combination of diminishing paramagnetic contributions of the Ln(III) ion at low temperatures, in addition to saturation effects arising from the large applied magnetic field (10 000 G) that could mask ferromagnetic interactions between the d/f metal ions; however, the same results as previously published where the $\chi_M T$ measurements decreased at lower temperatures for Ln = Dy(III) and Yb(III) were confirmed after repeating the $\chi_M T$ measurements at a lower magnetic field (500 G). The repeated experiments rule out the probability of the unprecedented interactions being a function of magnetic saturation. Thus, the cause of the antiferromagnetic behavior is still undetermined. This odd magnetic behavior of the $[LnNi_2(tam)_2]ClO_4 \cdot nH_2O$ complexes is puzzling due to the similarities of the H_3tam, H_3trn, and H_3bcn amine phenol ligands.

The only major difference between the trimetallic Ni−Ln−Ni structures is the variation in the intermetallic bond lengths. Shorter Ni−Ln and Ni−Ni intermetallic distances are observed for $[LnNi_2(bcn)_2]ClO_4 \cdot nH_2O$ compared to Bayly's Ni−Ln−Ni reduced Schiff base complexes[41] and Ōkawa's 2,6-di(acetoacetyl)pyridine systems (∼3.119 vs >3.53 Å for Ni−Ln distances; 5.98 vs >7.21 Å for Ni−Ni distances, respectively).[45] In addition, the Ni−Ni intermetallic distances for the $[LnNi_2(tam)_2]ClO_4 \cdot nH_2O$ complex were even shorter (∼5.4 Å). The shorter Ni−Ni distances for the $[LnNi_2(tam)_2]ClO_4 \cdot nH_2O$ complexes may give rise to an antiferromagnetic exchange between the two terminal Ni(II) species masking any weak ferromagnetic interaction between the Ln(III) and the terminal Ni(II) ions, observed between the terminal Ni(II) ions in the $[GdNi_2(bcn)_2]^+$ complex discussed herein. Unfortunately, attempts to remove the Ln(III) contributions of the $[LnNi_2(tam)_2]ClO_4 \cdot nH_2O$ have been unsuccessful due to failed efforts at synthesizing and crystallizing the analogous $[LnZn_2(tam)_2]ClO_4 \cdot nH_2O$ species.

Conclusion

A series of TM(II)−Ln(III)−TM(II) complexes were synthesized where a similar core structure of the complex was maintained regardless of the TM(II) or Ln(III) ion. $[TM(Hbcn)] \cdot nH_2O$, where the transition metal is encapsulated by the three amine donors and three phenolate donors, became a preorganized moiety used to sandwich the Ln(III) ion between the six donating phenolate oxygens, three from each $[TM(bcn)]^-$ ligand. Solvent molecules completed the large coordination spheres intrinsic to lanthanides, forming stable d/f/d complexes where the d- and the f-block metal ions are in close proximity, allowing the study of their magnetic exchange. Magnetic interactions in the $[LnNi_2(bcn)_2]ClO_4 \cdot nH_2O$ complexes were determined by removing the first-order orbital contributions of the Ln(III) determined by the analogous $[LnZn_2(bcn)_2]ClO_4 \cdot nH_2O$ species and analyzing their resulting $\chi_M T$ values using an empirical approach similar to the data analysis of Costes et al.[31] The $[LnNi_2(bcn)_2]ClO_4 \cdot nH_2O$ complexes displayed magnetic properties similar to those of other literature d- and f-block species despite different geometric demands, where an antiferromagnetic exchange was observed for the lighter Ln(III) (Ln = Nd(III)), while the heavier Ln(III) ions (Ln = Gd(III), Dy(III), and Yb(III)) exhibited ferromagnetic behavior. These conclusions are consistent with the predictions of Kahn et al.[44,46] where a ferromagnetic exchange is observed with $4f^n$ Ln(III) metal ions where $n > 7$ and an antiferromagnetic interaction arises if $n < 7$. This analysis is also used for the $[LnCu_2(bcn)_2]ClO_4 \cdot nH_2O$ species published in the following paper[50] allowing for the investigation of the magnetic behavior upon varying both TM(II) and Ln(III) while maintaining the same core structures. We remain hopeful that more trimetallic d/f/d literature examples with varied TM(II), Ln(III) and geometric demands will soon be synthesized and magnetically characterized to further understand the intrinsic d/f hetermetallic magnetic interactions.

Acknowledgment. We thank Dr. Cecilia Stevens for her expertise on magnetics and with the UBC SQUID. We acknowledge Discovery Grant support from the Natural Sciences and Engineering Research Council of Canada (R.C.T. and C.O.), a University Graduate Fellowship (C.A.B.) from the University of British Columbia, and a Royal Society Postdoctoral Fellowship (S.R.B.). We also acknowledge one of our reviewers for many helpful comments.

Supporting Information Available: Complete tables of crystal parameters, an ORTEP diagram of the cation in $[YbNi_2(bcn)_2]ClO_4 \cdot CH_3CN$, selected H^1 NMR spectra, selected IR data, and the temperature dependence plots of μ_{eff} for $[LnNi_2(tam)_2]ClO_4 \cdot nH_2O$ at 500 G, Ln = Gd(III), Dy(III), and Yb(III). This material is available free of charge via the Internet at http://pubs.acs.org.

IC701612E